COMPARATIVE STUDIES OF CELL PARAMETERS ON SYNTHETIC AND NATURAL MAGNETITE (Fe_3O_4) IN PRESENCE OF IMPURITIES.

BY

AGAJA A. SILAS B.Sc. (Hons)

A Thesis submitted to the Postgraduate School, Ahmadu Bello University, Zaria in partial fulfilment of requirements for the award of Master of Science Degree in Physics.

Department of Physics
Ahmadu Bello University,
Zaria.

March, 1992.

DECLARATION

I declare that this thesis has not been submitted in whatever form to any other institution, organization or body other than Ahmadu Bello University, Zaria, Nigeria for the award of any degree. Works of others consulted in the text have been accordingly referenced.

Agaja, S.A.

CERTIFICATION

This thesis titled Comparative studies of Cell Parameters on Synthetic and Natural Magnetite (Fe_3O_4) in presence of Impurities by Agaja Silas Adekoya, meets the regulations governing the award of the degree of Masters of Science of Ahmadu Bello University, Zaria, and is approved for its contribution to knowledge and literary presentation.

Prof. J. Adeniyi — Date: 20-12-92
Chairman, Supervisory Committee

(Dr. N. HARIHARAN) — Date: 21-12-1992
Member, supervisory Committee

Date: 20:12:92
Head of Department

Date: 23/8/94
Dean, Postgraduate School

ACKNOWLEDGEMENTS

My sincere gratitude goes to my supervisor Prof. J.A. Adetunji for his guidance, advice and patience through the period of the project. The contributions of the following people are thankfully acknowledged: Dr. and Mrs. Dim and Mr. David Barak.

I am grateful to the following people for their useful assistance and for the nice time we had together: K.I. Ibikunle, A.O. Mustapha, U. Joe, K. Usman and I. Kaka. To others who have contributed to the success of this thesis whose names are not mentioned due to space and time factor I am equally grateful for their efforts.

Finally, my profound gratitude to Almighty God for seeing me through the stormy days. And for making the most impossible become possible in my life.

DEDICATION

"To every struggling mind towards success".

ABSTRACT

X-ray diffraction Analysis (XRDA) for comparism between cell parameters of natural and four synthetic magnetite ($Fe_3{}^0{}_4$) (herein appropriately named after workers who provided the synthetization technique) have been carried out. The Energy dispersive-x-ray fluoresence (EDXRF) technique was used to find the contribution due to impurities on the cell parameters. The results obtained from the X-ray diffraction analysis of the samples revealed that the lattice constant, a, obtained for each of the method used are as follows: Natural sample ($a=8.398A^0$) Elmore sample (a=8.411A0, Haber sample (a=8.426A°) Lefort sample (a=8.411A°).

However, the results of the lattice parameter obtained for the samples show an increase of between 0.1% to 0.4%. when compared to those obtained by previous workers. Rooksby (1981) have shown that the lattice constant of 99"/. pure magnetite to be $8.396A^0$. Basta (1957) and O'Reilly (1967) have also determined the lattice parameters of magnetite to be $8.396A^0$.

The EDXRF analysis of the samples revealed that the following elements CI, K, Zn, Ca and Cu. were present as impurities both in the synthetic and Natural samples. The concentrations of these elements as well as the abundance percentage of iron in the samples were

determined. The influence of these impurity elements on the increase of the cell parameter is also discussed.

LIST OF TABLES

TABLE	TITLE	PAGE
4.1	Unrefined Bragg angle (θ) values for Natural sample	50
4.2	Unrefined Bragg angle (θ) values for Haber sample	50
4.3	Unrefined Bragg angle (θ) values for Baudisch/Welo sample	51
4.4	Unrefined Bragg angle (θ) values for Lefort sample	51
4.5	Unrefined Bragg angle (θ) values for Elmore sample	52
4.6	Refined Bragg angle (θ) values for Natural sample	52
4.7	Refined Bragg angle (θ) values for Haber sample	53
4.8	Refined Bragg angle (θ) values for Baudisch/Welo sample	54
4.9	Refined Bragg angle (θ) values for Leffort sample	54
4.10	Refined Bragg angle (θ) values for Elmore sample	54
4.11	Concentration of iron and impurities in Natural sample	57
4.12	Concentration of iron and impurities in Haber sample	58
4.13	Concentration of iron and impurities in Baudisch/Welo sample	58
4.14	Concentration of iron and impurities in Elmore sample	58
4.15	Concentration of iron and impurities in Lefort sample	59
4.16	Summary of lattice parameter values	59
4.17	Bragg angle (θ) with lorentz polarization factor values for Natural sample	60

4.18 Bragg angle (θ) with lorentz polarization factor values for Haber sample 60

4.19 Bragg angle (θ) with lorentz polarization factor values for Baudisch/Welo sample 61

4.20 Bragg angle (θ) with lorentz polarization factor values for Lefort sample 61

4.21 Bragg angle (θ) with lorentz polarization factor values for Elmore sample 62

LIST OF FIGURES

FIGURE	TITLE	PAGE
1.1	Spinel Structure ($MgAl_2O_4$)	6
1.2	Schematic representation of normal spinel structure	6
1.3	Crystal structure of magnetite (Fe_3O_4)	6
2.1	Schematic of an X-ray tube.	11
2.2	X-ray comtinuum from a target operated at voltages specified	11
2.3	Schematic illustration of the scattering of an incident wave	14
2.4	Instrumentation for X-ray spectroscopy.	17
2.5	Diffraction of X-rays from a set of crystal planes	21
2.6	Elimination of Zero error.	24
4.1	Bragg angle (2θ) peaks for Natural sample	39
4.2	Bragg angle (2θ) peaks for Haber sample	40
4.3	Bragg angle (2θ) peaks for Baudisch/Welo sample	41
4.4	Bragg angle (2θ) peaks for Lefort sample	42
4.5	Bragg angle (2θ) peaks for Elmore sample	43
4.6	Bragg angle (2θ) peaks for Silica Standard sample	44
4.7	$Sin^2\theta$ against Q^2 for Natural sample	45
4.8	$Sin^2\theta$ against Q^2 for Haber sample	46
4.9	$Sin^2\theta$ against Q^2 for Baudisch/Welo sample	47
4.10	$Sin^2\theta$ against Q^2 for Lefort sample	48
4.11	$Sin^2\theta$ against Q^2 for Elmore sample	49
4.12	Lorentz-polarization factor against Bragg angle (θ) for Natural sample	64
4.13	Lorentz-polarization factor against Bragg angle (θ) for Haber sample	65

4.14 Lorentz-polarization factor against Bragg angle (θ) for Baudisch/Welo sample 66

4.15 Lorentz-polarization factor against Bragg angle (θ) for Lefort sample 67

4.16 Lorentz-polarization factor against Bragg angle (θ) for Elmore sample 68

TABLE OF CONTENTS

TITLE		PAGE
Declaration		ii
Certification		iii
Dedication		iv
Acknowledgement		v
Abstract		via,b
List of tables		viia,b
List of figures		viiia,b,c
Table of Contents		ixa,b,c
CHAPTER 1		
INTRODUCTION		1
1.1.0	Spinel Structure	4
1.2.0	Inverse Spinel Structure	5
1.3.0	Structure of magnetite	7
CHAPTER 2		
2.0.0	X-ray fluorescence Analysis	9
2.1.0	Production of X-ray and X-ray spectra	12
2.2.0	X-ray diffraction analysis	14
2.2.1	X-ray diffraction	16
2.3.0	Instrumental Units	17
2.3.1	Collimators	19
2.3.2	Filters	20
2.3.3	Analyzing Crystal	20
2.4.0	Energy dispersive X-ray Fluorescence Spectroscopy (EDXRF)	22
2.5.0	Some sources of Errors in lattice constant determination	24

2.5.1	Eccentricity error	24
2.5.2	Absorption error	24
2.5.3	Zero error	25
2.5.4	Refraction error	25
2.5.5	Lorentz-Polarization error	26
2.6.0	Aims of the project	27
CHAPTER 3		
3.1.0	**EXPERIMENTAL PROCEDURE**	28
3.1.0	Methods of sample preparation	28
3.1.1	Leforts technique	28
3.1.2	Haber technique	28
3.1.3	Baudisch/Welo technique	29
3.1.4	Elmore technique	29
3.1.5	Natural technique	29
3.2.0	SAMPLE Analysis	30
3.2.1	X-ray diffraction analysis	30
3.2.2	Energy dispersive X-ray fluorescence Analysis (EDXRFA)	31
CHAPTER 4		
4.0.0	**RESULT AND DEDUCTIONS**	32
4.1.0	Refinement of 2θ values	32
4.2.0	X-ray diffraction results	32
4.2.1	Natural sample results	32
4.2.2	Haber sample result	33
4.2.3	Baudisch/Welo sample result	34
2.4	Lefort sample result	34
2.5	Elmore sample result	35
3.0	Graphical Calculation of cell parameters	36

4.3.1	Natural sample results	37
4.3.2	Haber sample results	37
4.3.3	Baudisch/Welo sample result	37
4.3.4	Elmore sample result	38
4.3.5	Lefort samplè result	38
4.4.0	Energy dispersive X-ray Fluoresence Result	55
4.4.1	Natural sample	55
4.4.2	Haber sample	56
4.4.3	Baudisch/Welo sample	56
4.4.4	Elmore sample	56
4.4.5	Lefort sample	57
4.5.0	Possition errors in relative intensity of diffraction patterns	62
4.6.0	Limitations and suggestions for future works	69
CHAPTER 5		
CONCLUSIONS		71
REFERENCES		73
APPENDICES		

CHAPTER ONE

1.0 INTRODUCTION

Magnetite (Fe_3O_4) is a ferromagnetic semiconductor, which is placed by crystallographers in their class 32 the members of' which are cubic structures, they posses the highest possible number of symeteries. The unit cell of magnetite Contain 32 oxygen ions in a face-centred cubic closed-packed arrangement (Verwey, et al, 1941). The cations occupy 8 tetrahedral and 16 octahedral interstices in the oxygen lattice. Simple ferrites show two variations: a normal spinel strucutre, where each type of ion occupies only one type of site and the inverse spinel structure, where both kinds of cations occur in the octahedral sites. Neutron diffraction measurements have confirmed the inverse spinel structure for magnetite (Shull et al, 1951).

It has been established that magnetite has the cubic inverse spinel structure (Verwey et al, 1939, 41). The explanation proposed for the high electrical conductivity of magnetite at room temperature ($10^{-2}\Omega$Cm) is that the distribution of ferrous and ferric ions among the octahedral cation lattice sites is random and fluctuating. That is, one can think of all 16 of these positions as being occupied by ferric ions, with 8 electrons continually changing their position from one site to another.

At room temperature, the magnetic properties of magnetite are quite similar to those of nickel. Its saturation magnetization (4.5 x 105 Amp/m) is about the same as for nickel, and, like nickel, its direction of easy magnetization is body diagonal [111] (Bickford, Jr. 1950).

The result of the torque measurement shows that, the magnetic symmetry changes from cubic above the transition to some form of uniaxail below the transition (Li, 1932). He also reported that if a single crystal had been cooled through the phase transition in a strong magnetic field, the direction along which this field had been applied become the direction of easy magnetization, or symmetry axis, below the transition.

The electrical resistivity increases abruptly upon cooling through the transition region (Okamura, 1932). In studying this effect Verwey (1941) and Haaman (1941) made extensive measurements on a series of sintered samples of varying composition. They discovered that both the transition temperature and the magnitude of the discontinuity in resistivity varied uniformly with the ratio Fe_2O_3/FeO. From this behaviour of the electrical resistivity, Verwey concluded that the distribution of ferrous and ferric ions among the octahedral lattice sites became ordered at the transition such an ordering implies that electronic interchange becomes more difficult, and the

resistivity, together with its activation energy, would be expected to increase. According, to this explanation, the phase transition is an order-disorder phenomenon. A theoretical explanation of this phase transition based on electron-electron correlation interaction has been developed (Cullen and Callen, 1970). This theory does not explicitly explain the lattice deformation Coexisting with the charge ordering. The importance of the electron-phonon interaction has been pointed out by some authors (Chakraverty, 1974, Sokoloff, 1972; Good enough, 1971 and Yamada, 1974) in connection with the uniform bulk distortion from the cubic to the orthorhombic system.

The heat capacity of magnetic at the Verwey transition also shows a λ-type anomaly (spliting of heat capacity curve into two at Verway transition) (Miller, 1919), and changes in unit cell and volume and crystal Symmetry (Bickford, 1953 and Hamilton, 1958). More recent measurements have, however, idicated considerably more complexity in phenomena occuring at the Verwey transition than previously thought. First of all, instead of one λ-type anomaly in the heat capacity versus temperature curve, two anomalies have been observed (Evans and Westrum 1972). Both the temperature and heat content of these anomalies depend on the amounts and kinds of impurities in Fe_3O_4 (Bartel and Westrum, Jr. 1974). Secondly, the lattice of the

low temperature phase is of lower symmetry than the orthorhombic or rhombohedral lattices deduced from ealier studies (Yamada et al, 1968).

Recently, Heat-capacity measurements have been reported (Koenitzer et al, 1989) for $Fe_3(1-\delta)O_4$ samples with δ =0 and 0.0049 in the temperature range 0.3 to 10k. Difference in heat-capacity curves have been shown. The Debye temperatures are 539k and 511k respectively.

SPINEL STRUCTURE

There are many class of inorganic crystals known as spinel, whose structure resemble that of mineral spinel itself, $MgALSO_4$. Fig. 1(a)) The general formular is represented by AB_2X_4. The unit cell contains thirty-two oxide ion in almost perfect cubic-close packed array and corresponds to the formula $A_8B_{16}O_{32}$. In the normal spinel structure the eight A ions occupy tetrahedral sites in the face centered cubic oxides and the sixteen B ions occupy the octahedral site Fig. 1(a).

The structure is closely related to those of sodium chloride (Nacl) and Zinc Sulphide (Zns). There are two major factors which determine the combinations of atoms that can form the spinel structured.

a) The total cation charges

b) The relative cation size

For oxide of the formular AB_2O_4, there are eight negative charges to be balanced, this can be achieved by the following three combinations of cation charges ($A^{2+} + 2B^{3+}$), ($A^{4+} + 2B^{2+}$) and ($A^{6+} + 2B^{+}$) they can be refered to as 2,3; 4,2 and 6,1 spinels structure respectively.

1.2 INVERSE SPINEL STRUCTURE

Many spinel compounds formed by the combination of ions do not have the normal spinel structure in which the A cations are occpued in the tetrahedral sites and B, cations and occupied in the octahedral sites, instead they adopt the inverse spinel structured in which the B cations tend to occupy the tetrahedral sites.

The following factors are usually taken into consideration before determining why some spinel tend to form the inverse spinel structure.

i) The relative sizes of A and B cations

ii) The medulung constants for the normal and inverse spinel structures.

iii) Polarization or Covalency effect.

According to radius ratio theory, the cations with radius ratio (ρ) in the range 0.144 - 0.732 prefer octahedral coordination while smaller cations with radius ratio between 0.225 and 0.414 would preferably occupy the tetrahedral sites. As trivalent cations B^{3+} are frequently smaller than divalent cations A^{2+} there

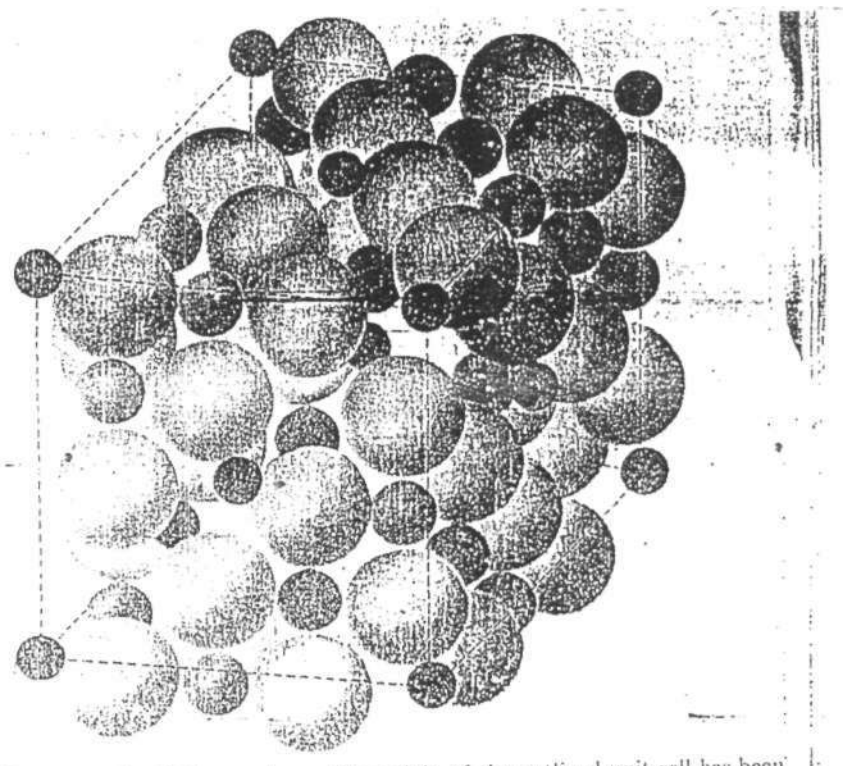


Fig. 11. Spinel ($MgAl_2O_4$) structure. The origin of the outlined unit cell has been placed in a tetrahedral void of the oxygen closest packing occupied by Mg.

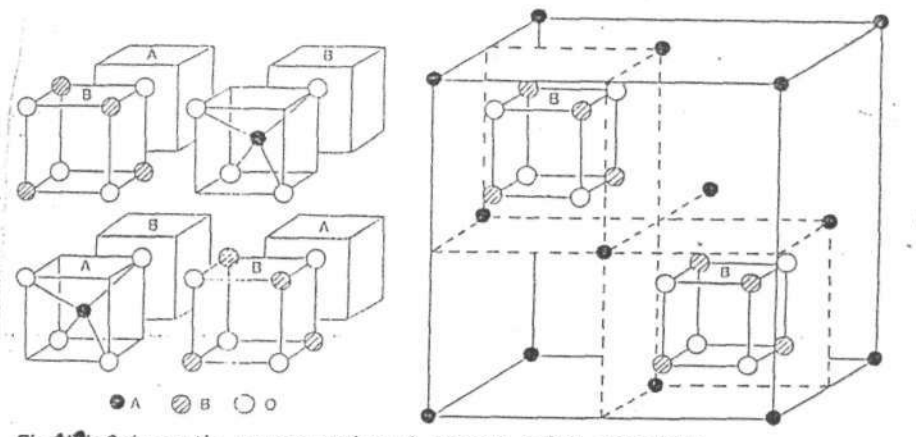


Fig. 11. Schematic representation of normal spinel structure

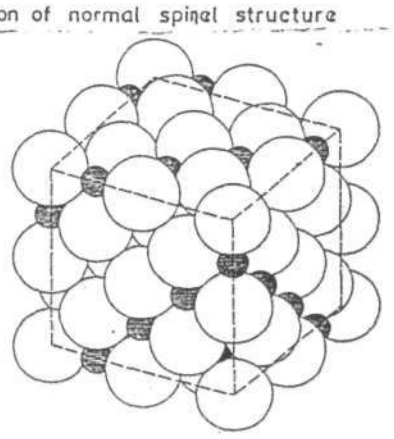


Fig. 13. Crystal structure of Fe_3O_4. Large open circles: oxygen ions at (idealized) 32-fold position; Small black circles: Fe^{3+} at 8-fold position (interstices between 4 oxygen); only one of these ions is visible; Medium-sized hatched circles: 16-fold position, containing both Fe^{2+} and Fe^{3+}, connected with the electronic conduction (interstices between 6 oxygen).

is tendency for them to occupy the tetrahedral sites.

1.3 STRUCTURE OF MAGNETITE

Magnetite (Fe_3O_4) is a mixture of Fe^{2+} and Fe^{3+} oxide which occurs in nature in the form of black, octahedral crystals of the mineral magnetite. The Fe^{2+} ions are all in octahedral interstices, whereas the Fe3+ ions are half in tetrahdral and half in Octahdral interstices of a cubic close-packed array of oxide ions Fig. 1 (b).

The tendency of each of these oxides to be non-stoichiometric is due to some extent the intimate relationship between their structures. The structure may be visualized by starting with a cubic close-packed array of oxides ions and distributing a certain number of Fe^{2+} and/or Fe^{3+} ions among the octahedral and tetrahedral holes. Thus, when all of the octahedral holes are filled by Fe^{2+} ions, one has the ideal FeO structure. If a small portion, of these 3δ Fe^{2+} ions are replaced by 2/3 their number of Fe^{3+} ions, one gets the usual defect structure for ferrous oxide, for example, $Fe_{(1-\delta)}O$, where δ is commonly 0.05. If this process is contined until 2/3 of the iron atoms Fe^{3+} and half of these migrate to tetrahedral sites, Fe3O4 conversion of the remaining Fe^{2+} to Fe^{3+} gives γ - Fe_2O_3. The fact that each of these oxides can alter its composition in the direction of one or two of the others without, there being any major structural

change but only a redistribution of ions among the tetrachedral and octahedral interstic es accounts for their nearly interconvertibility, their tendency to be non-stoichiometric.

CHAPTER TWO

2.0 X-RAY FLUORESCENCE ANALYSIS

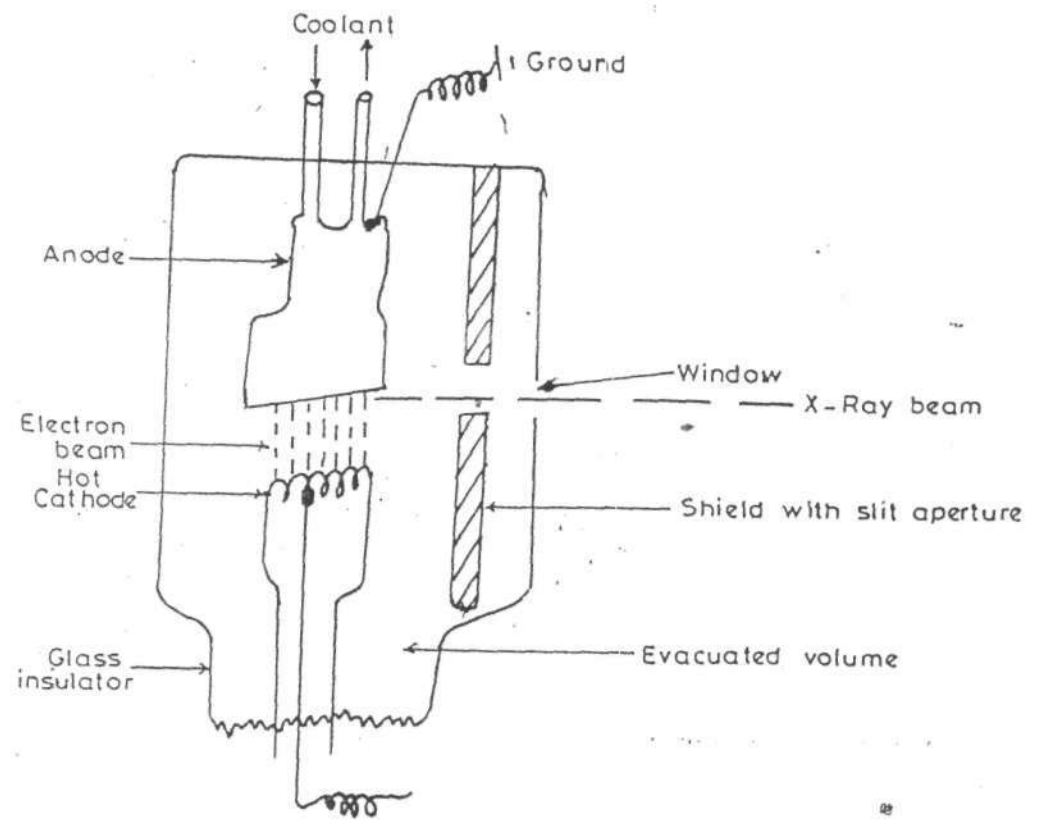
Following the discovery of X-rays in 1895 by Wilhelm Roetgen, use of X-ray techniques based on properties of X-rays has played an increasingly important part in materials characterization and analysis.

X-rays are electromagnetic radiation and are manifested in two forms, continuous radiation and characteristic radiation. Continuous radiation is produced when a high-energy electron beam decelerates as it approaches the electron clouds that surround the atomic nucleus. Characteristic radiation is produced following the ejection of an inner orbital electron by high energy particles and subsequent transition of atomic orbital electrons from states of high to low energy. In 1912, Moseley showed that the relationship between the emission wavelengths and the atomic number of excited element is $E = \frac{1}{\lambda} = K (Z-S)^2$, Z=atomic number, K and S are constant which depend on the spectral series of the emission line in question.

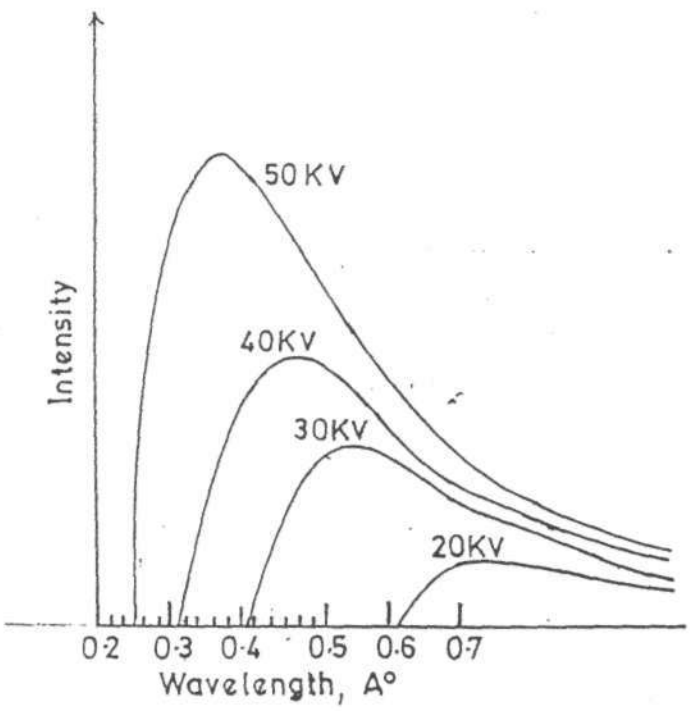
After the demonstration of the diffraction of X-rays by Mas Von Laue in 1912, two major fields of materials analysis have developed. X-ray emission spectrometery is a technique for qualitative and quantitative elemental analysis by measurement of the wavelengths and intensities of X-rays from th excited elements. The second technique is X-ray diffraction,

which is a means of materials characterization. In the X-ray scattering characteristics of a substance are related to the molecular arrangement of the atoms making up the scatterer.

X-ray emission spectrometry, is the use of primary X-rays to excite characterstic secondary radiation from the specimen being analyzed. The technique is therefore referred to as X-ray fluorescence spectrometry. X-ray fluorescence spectrometry uses either the diffracting power of a single crystal to isolate narrow wave-length band or a proportional detector to isolate narrow energy bands from the polychromatic beam of characteristic radiation excited from the sample. The first of the methods is called wavelength-dispersive spectrometry, and the second, energy-dispersive spectrometry. Because of the known relationship between emission wavelength and atomic number, isolation of individual characteristic lines allows the unique identification of an element to be made, and elemental concentrations can be estimated from characteristic line intensities. Thus, this technique is a means of materials characterization in terms of elemental composition.



FIG·2·1: SCHEMATIC OF AN X-RAY TUBE



FIG·2·2: X-RAY CONTINUUM FROM A TARGET OPERATED AT VOLTAGES SPECIFIED

2.1.0 PRODUCTION OF X-RAYS AND X-RAY SPECTRA

An X-ray tube is basically a large vacuum tube cotaining a heated cathode (electron emitter) and an anode. Electrons emitted by the cathode are accelerated through a high-voltage field between the target and cathode. Upon impact with the target, the stream of electrons is quickly brought to rest. The electrons transfer their kinetic energy to the atoms of the material making up the target. Part of the kinetic energy is emitted in a continuous spectrum of X-rays covering a broad wavelength range (Fig. 2.2) with a broad maximum in intensity and falling off to a definite short-wavelength limit. The broad range of x-ray photon energies is due to deceleration of impinging electrons by successive collisions with the atoms of the target material. Consequently, the emitted quanta are of longer wavelength than the short-wavelength cut-off, λ_0, which is independent of the target element and depends upon the voltage across the X-ray tube. At the cut-off wavelength all of the energy of the electron is converted, at one impact, to a photon. The relationship between the voltage and is given by Duane-Hunt equation

$$\lambda(\text{Å}) = \frac{hc}{eV} = \frac{12400}{V}$$

V = X-ray tube voltage in volts

e = charge on electron

h = planck's constant

c = velocity of light

An increase in the tube voltage results in an increase in the total energy emitted and a movement of spectral distribution toward shorter wave-length. The wavelength of the maximum intensity is about 1.5 times short-wavelength limit. The intensity of the spectrum increases with atomic number of the target element.

If sufficient energy is available, the transfer of energy from the impinging electron beam may eject an electron from one of the inner shell of atoms consituting the target material. The place of the ejected electron will then promptly be filled by an electron from an outer shell whose place, in turn, will be taken by an electron coming from still further out. Thus, the ionized atom returns to its normal state in a series of steps in each of which an X-ray photon of definite energy is emitted. These transitions give rise to the characteristic line spectrum of the material in the anode or of a specimen pasted on the target. When originating in an X-ray tube, their lines will be superimposed on the continuum. The k series of lines is observed when an electron in the inner most k shell is dislodged; it arises from electrons droping drown from L to M oritals into the vacancy in the k shell. Corresponding vacances in the L shells are filled by electron transitions from outer shells and give rise to the L series.

2.2.0 X-RAY DIFFRACTION ANALYSIS

This method depends upon the wave character of X-ray and regular spacing of planes in a crystal discussed in section 2.00 and 2.1.0. Although, diffraction methods can be used for quantitative analysis, they are most widely used for qualitative, identification of crystalline phases.

DIFFRACTION EQUATIONS

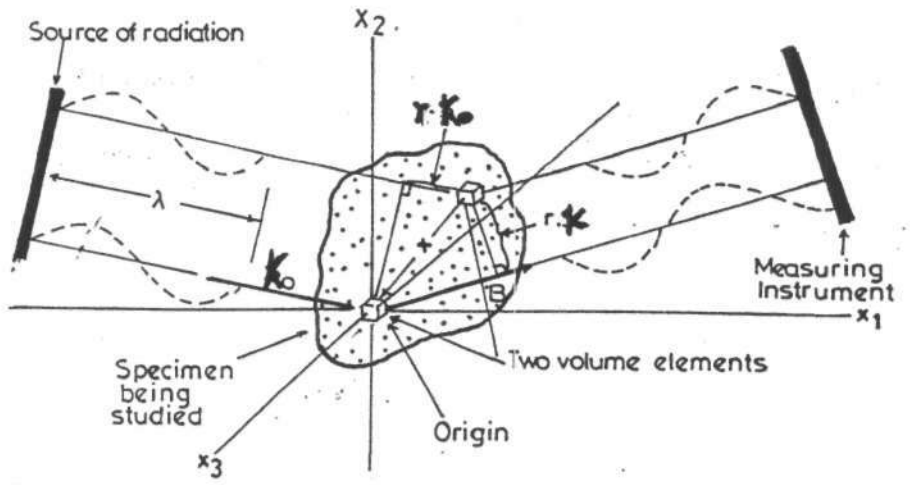


Fig. 2.3 illustrates the schematic scattering of an incident wave Ko by two volume elements to produce the coherently scattered wave k observed at the location of the measuring instrument.

In most diffraction experiments a parallel beam having a wavelength and with all wavelets in phase strikes the specimen in a direction specified by the unit vector Ko. Some of the energy of the wave transfers without loss to the material of the specimen, this material then becomes a scattering centre for

radiation of the same wavelength and phase as the incident radiation, a process known as coherent scattering. The scattered waves radiates in all directions, if the measuring instrument registers only the intensity of scattering in the direction specified by the unit vector k. The phase difference is $\frac{2\pi}{\lambda}(k-Ko).r$. This expression can be witten as $2\pi K'.r$ where $K' = (K-Ko)/\lambda$. With reference to the amplitude of the wave scattered at the origin, the amplitude dA(s) scattered by the volume element dV at r is

$$dA(k) = \rho(r)\ \mathrm{Exp}\ (-2\pi i k'.r)\ dV \quad \ldots\ldots \text{Eqn. (2.1)}$$

The minus sign occurs because of the definition used for path length. The quantity $\rho(r)$ is a more suitable measure of the effectiveness with which the material in the volume dV at the end of vector r scatters the incident wave. For all the volume element in the specimen eqn 2.1 becomes

$$A(k) = \int \rho(r)\ \mathrm{Exp}\ (-2\pi i k'.r)\ dV \quad \ldots\ldots \text{Eqn 2.2}$$

This equation is very convenient for two reasons. First, the intergral is a well-known quantity, the fourier transform of the function $\rho(r)$; numerous tables give the Fourier transform A(s) for various values of $\rho(r)$. Secondly, the vector K that determines the emplitude is not in the crystal but is referred to the reciprocal lattice (the inverse relation between the spacing of the points and the planes given rise to them).

Therefore, once we know the amplitude function (As) in the reciprocal lattice, we can predict the type of diffraction effect that will be observed for any particular type of diffraction experiment.

2.2.1 X-RAY DIFFRACTION

When X-rays are used for diffraction studies, various factors must be considered, but the essential one is the scattering effectiveness $\rho(r)$ of the material being studied. Scattering of X-rays is caused by the electrons in the atoms, and therefore, $\rho(r)$ increases directly with atomic number (Z). When scattering is referred to that produced by a single electron, the atomic scattering factor F (k) is equal to Z at $\theta=0$, although, it drops off as $(\sin\theta)/\lambda$ increase. A(k) is identical to $A(k)$ for a structure consisting of one atom of same kind per unit cell. If the unit cell contains N atoms, each located by the vector kr, then the structure factor, F(k) = A(k) is given interms of the miller indices (h k l) as.:

$$F_{hkl} = \sum_{r=1}^{N} f_r \, Exp\,2\pi i(hx_r + ky_r + lz_r) \cdots Eqn.\ 2.3$$

This can also be written as

$$F_{hkl} = \sum f_r \left\{ Cos\,2\pi(hx_r + ky_r + lz_r) + i\,Sin\,2\pi(hx_r + ky_r + lz_r) \right. \cdots Eqn.\ 2.4$$

If there is a centre of symetery at the origin of the unit cell, then for every atom with coordinates X_r, Y_r, Z_r there is an identical atom at $-X_r$ $-Y_r$ $-Z_r$ and Since Sin (-X) = -Sin(x), the imaginary part of Eqn 2.4 vani'shes.

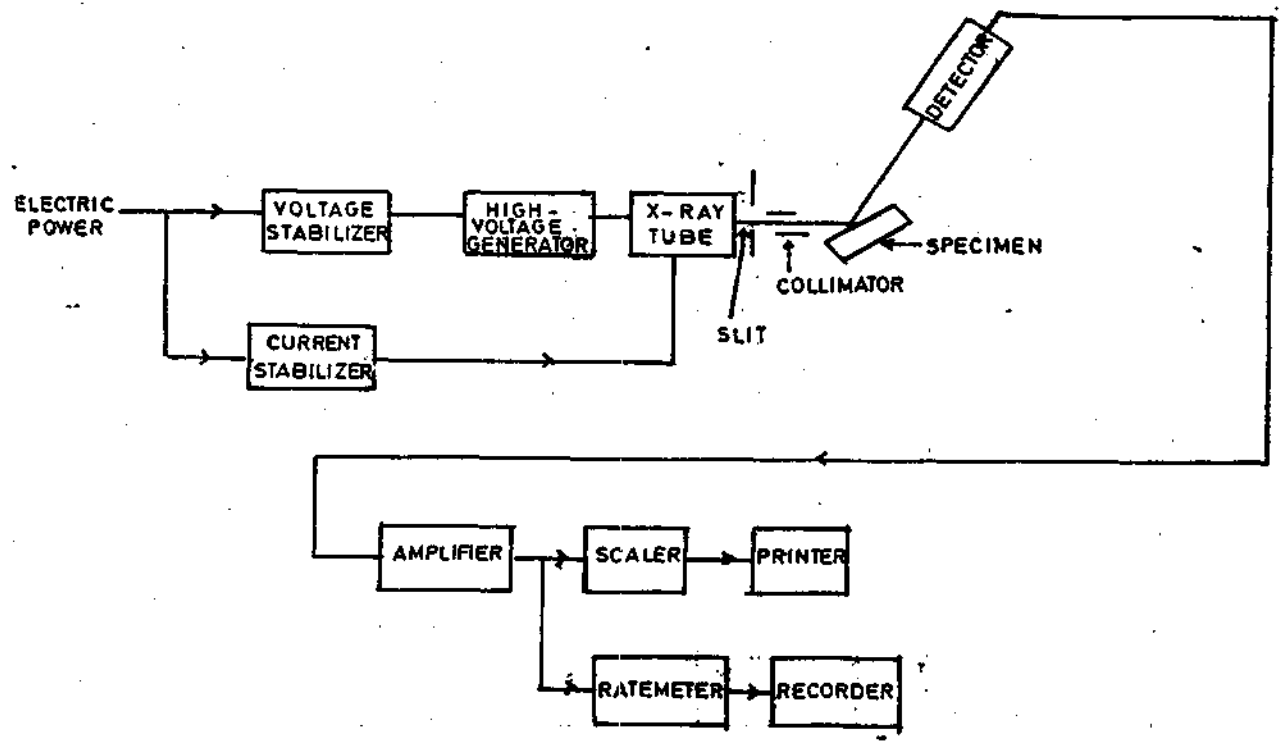
$$F_{hkl} = \sum_{r=1}^{N} f_r \cos 2\pi (hx_r + ky_r + lz_r) \cdots \text{Eqn. 2.5}$$

For a non-centrosymetric crystal Eqn 2.5 must be used. For the centrosymmetric crystal Eqn 2.4 is suitable. If only one of each pair of centrosymmetrically related atoms is included in the summation, the expression may be written as

$$F_{hkl} = 2 \sum_{r=1}^{N/2} f_r \cos 2\pi (hx_r + ky_r + lz_r) \cdots \text{Eqn. 2.6}$$

2.3.0 INSTRUMENTAL UNITS

Instrumentation associated with X-ray methods is general is outline schematically below Fig. 2.4.



FIG·2·4 : INSTRUMENTATION FOR X-RAY SPECTROSCOPY

The modern X-ray tube is a high-vacuum, sealed off unit, usually with a copper or molybdenum target, although targets of chromium, iron, nickel, silver and tungsten are used for special purposes. The target is viewed from a very small angle above the surface. If the focal spot is a narrow ribbon, the source appears very small when viewed from the end, which leads to the sharper definition demanded in diffraction studies. Because it becomes hot, the target is cooled by water and is sometimes rotated when a very intense X-ray beam is generated. The X-ray beam passes out of the tube through a thin window of beryllium or a special glass. For wavelengths from 6Å to 70Å . Ultra thin films (1-m aluminium or cast parlodion films), separate the X-ray tube from the remainder of the equipment, which must be evacuated or flushed with helium.

Associated equipment modules high-voltage generators and stabilizers. Voltate regulation is accomplished by regulating the main A.C supply. Current regulation is accomplished by monitoring the D.C. X-ray tube current and controlling the filament voltage. Either full-wave rectification or constant high potential may be used to operate the X-ray tube. In full-wave rectification the voltage reaches its peak value 120 times a second but only persist at that value for a small fraction of time, constant high potential, obtained through electronic filtering, increases the output of characteristic X-rays from a specimen,

particularly with elements emitting at short wavelengths. With a tube operated at 50 kV the gain is two fold for elements up to about atomic number 35 (Br), increasing to fourfold for atomic number 56(Ba). Commonly, X-ray tubes are operated at 50 to 60 kV. Tubes of 100kV rating are available and extend the range of elements whose k series can be excited and the sensitivity, because on increasing the voltage the intensities of all line increase.

2.3.1 COLLIMATORS

Radiations from an X-ray tube is collimated either by a series of closely spaced, parallel metal plates or by a bundle of tubes, 0.5mm or less in diameter. In a fluorescence spectrometer, one collimator is placed between the specimen and the analyzer crystal to limit the divergence of the rays that reach the crystal. The second collimator, usually coarser, is placed between the analyzer crystal and the detector where it is particularly used at very low goniometer angles for preventing radiation that has not been reflected by the crystal from reaching the detector. Increased resolution can be obtained by decreasing the separation between the metal plates of the collimator or by increasing the length of the unit, but this is achieved at the expense of intensity.

2.3.2 FILTERS

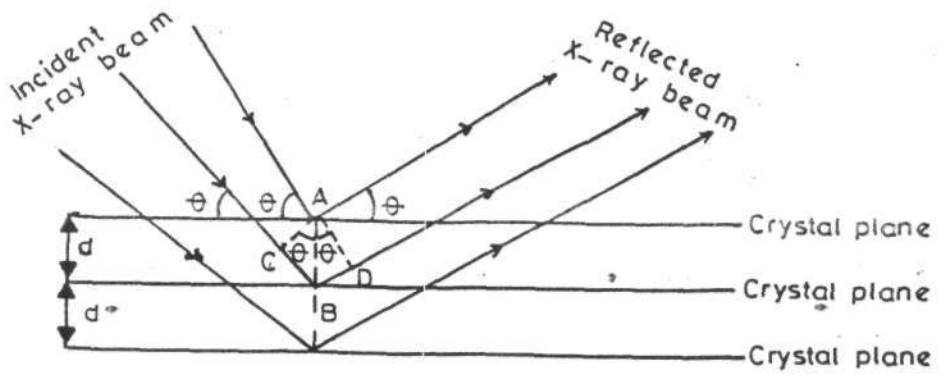
When the wavelengths of two spectral lines are nearly the same and there is an element with an absorption edge at a wavelength between the lines, that element may be used as a filter to reduce the intensity of the line of shorter wavelength. In X-ray diffractometer it is common practice to insert a thin foil in the primary X-ray beam to remove the k line from the spectrum while, transmitting the K lines with a relatively small loss of intensity. The Background radiation (the continuum) is reduced by the same method.

2.3.3 ANALYZING CRYSTAL

Virtually, monochromatic radiation is obtained by reflecting X-rays from crystal planes. The relationship between the wavelength of the X-ray beam, the angle of diffraction θ, and the distance between each set of atomic planes of the crystal lattice d is given by Bragg condition.

$$m\lambda = 2d\sin\theta \qquad \text{... Eqn 2.7}$$

where m represent the order of diffraction. The geometrical relations are shown below:



FIG·2·5;DIFFRACTION OF X-RAYS FROM A SET OF CRYSTAL PLANES

For the ray diffracted by the second plane of the crystal, the distance CBD represents the addtional distance of travel in comparison to a ray reflected from the surface. Angles CAB and BAD are both equal to θ.

Therefore, CB = BD = AB Sinθ

and CBD = 2AB Sinθ.

where AB is the interplanar spacing, d. In order to observe a beam in the direction of the diffracted rays, CBD must be some multiple of the wavelength of the X-rays such that the diffracted waves will be in phase. The angle between the direction of the incident beam and that of the diffracted beam is 2θ. In order to scan the emission spectrum of a specimen, the analyzing crystals is maunted on a goniometer, an instrument for measuring angles, and rotated through the desired angular region.

The range of wavelenghts usable with various analyzing crystal is govern by the d-spacing of the crystal planes and by the geometric limits to which the

goniometer can be rotated. The d value should be small enough to make the angle 2θ greater than approximately 8° even at the shortest wavelength used, otherwise excessively long analyzing crystals would be needed in order to prevent the incident beam from entering the detector. A small d-spacing is also favourable for producing a larger dispersion, $\frac{\partial\theta}{\partial\lambda}$ of the spectrum as can be seen by differentiating the Bragg equation.

$$\frac{\partial\theta}{\partial\lambda} = \frac{n}{2d\cos\theta} \quad \text{..... Eqn. 2.8}$$

On the other hand, a small d-value imposes an upper limit to the range of wavelengths that can be analyzed, because $\lambda = 2d$ the angle 2θ becomes 180°. Actually, the upper limit to which goniometers can be rotated is mechanically limited to a 2θ value of around 150°. For longer wavelengths a crystal with a large d-spacing must be selected.

2.4.0 ENERGY-DISPERSIVE FLUORESCENCE SPECTROSCOPY (EDXRF).

The basis of the X-ray fluoresence technique has been explained in section 2.0.0. The instrumental units of the energy-dispersive spectrometer consist of three basic units, an excitation source, a spectrometer, and a detection system. In this case, the detector itself acts as the dispersion agent. The

detector is generally a lithium-drifted silicon, Si(Li) detector, which is a proportional detector of high intrisic resolution.

EDXRF has been distinguished as a simple and versatile analytical method with many advantages over other methods, including fast and simultaneous detection of all elements in the sample with Z>15 regardless of their chemical form, non-destructiveness and easy for sample preparation. EDXRF analysis can be divided into three steps.

Qualitative analysis of peak identification. This is usually not a problem because X-ray spectra are relatively simple; i.e. every element is represented with only few characteristic lines, while overlapping effect are rare.

Spectrum analysis or determination of characteristic peak intensities is usually performed by some least squares fitting procedure.

Quantiative analysis, i.e. conversion of measured intensities into corresponding mass concentrations, taking into account the nature and abundance of all other elements in the sample (Orlic et al, 1988).

2.5.0 SOME SOURCES OF ERROR IN LATTICE CONSTANT DETERMINATION

The angle of diffraction 2θ mentioned in Sec. 2.3.3 can not be easily measured absolutely. Some errors usually associate with the 2θ values. The errors and possible ways of minimizing them are discuss below:

2.5.1. Eccentricity Error.

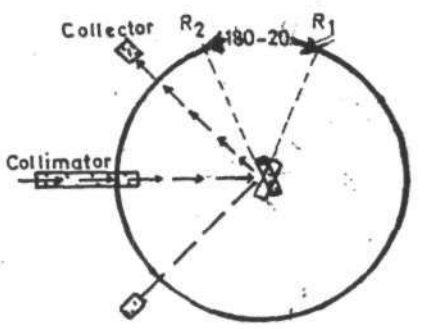


FIG. 2.6 : ELIMINATION ZERO ERROR

If the crystal, Fig. 2.6 is off the center, the beam does not follow the paths as shown in Fig. 2.6 and this causes the beam angles to be read wrong. However, if one uses large windows in the counting tubes the crystal angles with the collimated beam are still correct and can be read accurately.

2.5.2 Absorption error.

Absorption merely displaces the beam it affects the apparent beam angle but not the crystal angle at reflection (Bond 1959). If measurement is made

between the reflected beams both eccentricity and absorption causes errors, while if one measure between crystal positions neither of these causes errors.

2.5.3 Zero Error

Fig. 2.6. If the reading of the crystal position on a divided circle for one position, say R_1, is noted, and then noted the reading R_2 for the second. It is readily shown that for $R_2 > R_1$ and R = 0 not between R_1 and R_2:

$$\theta = 90^{o} - (R_2 - R_1)/2 \quad \text{..... Eqn 2.9}$$

if R = 0 lies between R_1 and R_2 one will need to modify Eqn. 2.9. to:

$$\theta = (R_2 - R_1)/2 - 90 \quad \text{..... Eqn. 3.0}$$

This method of determining θ eliminates zero error.

2.5.4 Refraction Correction

A correction must be made for refraction. If the diffraction is from a flat surface parallel to the atomic reflecting plane the correction given by (Compton and Allison, 1935) is made by the equation.

$$d = d'(1 + \delta/\sin 2\theta) \quad \text{... Eqn. 3.1}$$

The same reasons used in deriving eqn 3.1 shows that if the surface is not parallel to the reflecting planes about the measuring axis by amount ε the

correction is made by the equation:

$d = d\,(1 + \cos\varepsilon)/[\sin(\theta+\varepsilon)\sin(\theta-\varepsilon)]$. Eqn. 3.2

If $\varepsilon \ll \theta$, eqn. 3.7 gives the same results as Eqn. 3.2.

δ is unity minus refractive index of the crystal for the X-ray wavelength used.

$$\delta = ne^2\lambda^2/(2\pi mc^2) \quad \ldots \text{ Eqn. 3.3}$$

where e is charge on electron, m its mass, c is the velocity of light, and n is the number of electrons per cm^3. (Richtmeyer and Kennard, 1947).

2.5.5 Lorentz-Polarization error

Another source of error to be considered is the displacement of the response curve peak due to the Lorentz and polarization factors. For points near the peak θ_p let $X = \theta - \theta_p$ and write the curve as the cauchy curve,

$$y = A\{1 + (2x/w)^2\}^{-1} \quad \text{Eqn. 3.4}$$

where w is the width at half maximum. Eqn. 3.4 can be written as:

$Y' = Ly$ where $L = (1 + \cos^2 2\theta)/(2\sin 2\theta)$ ... Eqn 3.5 is the lorentz polarization factor.

$$\frac{dy'}{dx} = L\frac{dy}{dx} + y\frac{dL}{dx} \quad \ldots\ldots \text{Eqn. 3.6}$$

vanishes at θ_p, x is given by

$$\frac{1}{y}\frac{dy}{dx} = -\frac{1}{L}\frac{dL}{dx} \quad \ldots\ldots \text{Eqn. 3.7}$$

As the peak is displaced less than the half width the factor $(2x/w)^2 << 1$. Hence

$$x = w^2 [Cot2\theta/4 + Sin\ 4\theta/[2(1 + Cos^2 2\theta)] \quad \text{Eqn. 3.8}$$

The absolute value of x is to be added to θ. It is generally very small at large values of θ.

2.6.0 AIMS OF THE PROJECT

i) To prepare magnetitie as proposed by Lefort (1925), Elmore (1938), Baudisch/Welo (1925) and Haber (1925).

ii) To determine and compare the cell parameters of each of the methods in (1) with natural sample using X-ray diffractometer.

iii) To determine and compare the concentration of iron content in each of the sample mentioned in (i) with the natural sample

iv) To determine the impurities and their concentrations in both synthetic and natural sample.

v) To investigate the effect of the impurities in (iv) on the lattice constant.

CHAPTER THREE

EXPERIMENTAL PROCEDURE

3.1.0 Methods of sample preparation.

The various methods used to prepare the magnetite samples are discussed in the following sections.

3.1.1 Lefort's. 19.4 gm of $Fe_2(SO_4)_3.10H_2O$ and 13.4gm of $FeSO_4.7H_2O$ are separately disssolved in 75cc and 50cc of water, repsectively. They are then mixed and poured into a boiling solution of NaoH containing 25gms of the hydroxide in 320cc of water. The black mixture formed on the addition of sulphates is boiled for an hour. The precipitate was alternatively filled with water and was centrifuge until the washings become neutral forwards litmus paper. The precipitate was dried in an evacuated disicator. When finally dried it breaks up into brittle cakes or lumps which was ground into a fine powder.

3.1.2 Haber's Method. 176gm of a 25per cent. solution of ammonia are added to a 2.2 litres of a 10 per cent solution of crystalline ferrous sulphate and the mixture was boiled to the boiling point. While the mixture was boiling, 25.5gm of KNO_3 dissolved in a little water as possible was poured in. Boiling was continued for 15 minutes. This material settles rapidly and is easily decanted and washed without use of the centrifuge. the magnetite dries rapidly and does not shrink and cake on drying. In order words, the

concept of coagulation is not prominent in this method of preparing magnetite.

3.1.3. The Baudisch and Welo Method. 2.6gm of NaoH and 2gm of KNO_3 are dissolved in 0.5 litre of water. To this solution is added 9 gm $FeSO_4.7H_2O$ dissolved in 50cc of water. The solution is first greenish and finally becomes black. The precipitate settles rapidly and is easily washed and dried.

3.1.4 Elmore's method. 2.8gm of ferrous sulphate and 4 gm. of ferric sulphate was dissolved in 300cc of hot water. To this solution was added 5gm of NaoH dissolved in 50cc ofwater, with constant stirring. The solution was then filtered to remove salt and excess NaoH. The resulting precipitate was washed several times with water and finally with 0.01N Hcl. This was finally dried in the desicator.

3.1.5. Natural magnetite. The natural magnetite was obtained from iron-ore deposit at Itakpe-Okene in Kogi state. The natural magnetite was grinded gently with an augite morta into fine powder in the presence of acetone in order to have a better homogeneous sample. The magnetite part of the sample was removed with the aid of a magnetic separator at Geology department of A.B.U., Zaria. This was done by scanning through the sample several times.

The methods used to prepare the synthetic samples

were adopted because of the availability of the oxides and equipments required for the magnetite preparation. However, other methods such as: hydrothermal growth and skull melting technique can be used but the oxides and equipments required for the later methods were not available.

3.2.0 SAMPLE ANALYSIS

3.2.1 X-RAY DIFFRACTION ANALYSIS (XRD)

The samples described in Sec (3.2.1 - 3.2.5) were grinded gently and carefully into fine powder with an augite mortar this was to ensure that the symetricaly arrangements of the lattice was not distorted. The powdered sample was put into an aluminium holder to obtain clear diffraction patterns free of abnormally broadened and divergent diffraction peaks with respect to intensity distribution. The sample was mounted appropriately and proper allignment of the sample and the X-ray tube was ensured. The goniometer and the chart recorder were also set appropriately to ensure proper scanning and plottings of the diffracted X-rays. Each sample was scanned between (0.3^{o} to 80^{o} 2θ).

The experiment was carried out using the phillips type PW1390 X-ray diffractometer under the following working conditions.

i) Low temperature

ii) Radiation Cuk_{α}

iii) Energy of Copper E Cuk_{α} = 8040eV

vi) Tube high tension (Operating voltage) = 40kv

v) Tube current (operating current) = 30mA

vi) X-ray wavelength = 1.5418 A°

vii) Channel control gain = 32

viii) Channel control range = 2 x 10^{4}Hz

ix) Chart recorder speed = 0.2 cm/min

x) Scanning speed = 0.25°/min

xi) Take off angle = 0.3°

3.2.2 ENERGY DISPERSIVE X-RAY FLUORSCENCE ANALYSIS (EDXRF)

The purity of the powdered samples described in Section (3.2.1 - 3.2.5) were studied using the Energy dispersive X-ray fuoresence (EDXRF). The work was done in Centre for Nuclear Science Techniques, University of Nairobi, Kenya.

The powdered magnetite (Natural and synthetic) were smeared on glue of scotch tape measuring about 2.5cm x 3.0cm using non-fibrous paper. The sample was exposed to CD-109 sources for times ranging from 500-1000 secs. The resulting data was collected with the series 40 MCA. The data was transfered for processing using IAEA soft ware (XREA) for intensity determination. The determined intensity were used to calculate the concentration in percentage of the various elements present the calculations and results is discussed in Section (4.2.1 - 4.2.5).

CHAPTER FOUR

4.0.0 RESULTS AND DEDUCTIONS

The results of the X-ray diffraction (XRD) and Energy dispersive X-ray fluoresence analysis of the natural and synthetic samples discussed in chapter three is presented thus:

4.1.0 Refinement of 2θ values for the sample

The 2θ values obtained for the samples Fig. (4.1 to 4.5) were corrected for by scanning also for the standard (Silica), the recorded 2θ positions of the prominent peaks were noted fig 4.6 and compared with the values obtained from ASTM X-ray data file. Any systematic error, either possitive or negative is noted and used to correct the 2θ values obtained for the other samples. However, the silica standard and the samples were scanned on same single sheet of paper and the alignment of the goniometer and other working conditions of diffractometer remain the same to ensure accurate result.

4.2.0 X-ray diffraction results

4.2.1 Natural sample: The result of the diffracted X-ray peaks for the natural sample is shown in Fig. 4.1. Most of the prominent peaks occured between (23^{o} to 65^{o}, 2θ). The relative intensity for each of the angles is determined by counting the number of squares under the graph that each peak occupied and dividing it

by a background. Table 4.1 gives the summary of the respectives angle of diffraction θ, interplannar spacing, relative intensities and the Miller indices associated with each angle.

The lattice parameter for these set of diffraction angle was determined by using the Bragg's Law $2d_{hkl} \sin\theta = n\lambda$. The calculation was done using the computer programme in pascal shown in appendix (A1). The result of thelattice parameter calculated gave a value of 8.403A° with θ unrefined while the θ refined data gave 8.398A° for the natural sample. If this values were compared to 8.396A° earlier obtained by Basta and O'Reilly (1967) for magnetite, there is a difference of 0.007A° and 0.002A° respectively. The difference could be due to inherent impurities in the sample the presence of which was confirmed by the EDXRF analysis (See. 4.2.0).

4.2.2 . Haber's methods: The result of the X-ray diffracted angles for this sample is shown in Fig. 4.2, Table 4.2 shows the diffracted angles, interplanar spacing, the relative intensity and the Miller indices of each diffracted angles. The lattice parameter was calculated for this sample using the computer programme in pascal in Appendix (A1). The values obtained for the cell parameter was 8.451A° with θ unrefined data while the θ refined data gave 8.426A°. This shows an increase of 0.055A° and 0.030A° respectively, when compared to 8.396A° obtained by Basta (1967) the

increament in the cell parameter is most likely due to the presence of impurities in the sample.

4.2.3. Baudisch/Welo method: The result of the X-ray diffracted angles for this sample is shown in Fig. 4.3. While, table 4.3 shows the respective Bragg angles, interplannar spacing, relative intensity and the miller indices. The cell parameter was calculated for this sample, using the computer programme in appendix (A1). The lattice constant obtained was 8.443A^{o} with θ unrefined data while, the θ refined result gave 8.411A^{o}. The values shows an increase of 0.047A^{o} and 0.0125A^{o} when compared with 8396A^{o} obtained by Basta (1967). The increament in cell parameter is associated with the presence of the impurities in the sample.

4.2.4 Lefort method: The result of the X-ray diffracted peaks was shown in Fig. 4.4. Table 4.4 shows the X-ray diffracted angle, interplanar spacing, relative intensity, and the Miller indices. From fig. 4.4 it can be observed that the resolution of the diffracted peaks is very poor when compared to the peaks obtained for previous samples. This is due to the fact that in Lefort's method the FeO content is less than two-thirds that of Haber's and Baudisch and Welo. This is an indication that the Crystals in Lefort's magnetite are smaller and they are exposed to

a relatively larger surface for oxidation and other actions of the nature of surface phenomena.

However, the lattice constant calculated was 8.438A° with the θ unrefined data while, θ refined was 8.423A°. If this values were compared with 8.396A° obtained by Basta (1967) it shows an increament of 0.042A° and 0.027A°. This is due to the impurities in host lattice.

4.2.5 Elmore method: The result of the X-ray diffraction peaks for this sample is shown in fig. 4.5 and table 4.5. From fig. 4.5 it can be seen that the resolution of the peaks resembles those of leforts sample this is due to similarity in the mode of their sample preparation. Therefore, the same reasons given for the lefort sample is still applicable to this sample in order to account for the poor resolution of the peaks.

The lattice parameter was calculated using the computer programme of appendix (A1). 8.410A° was observed as the cell parameter with the θ unrefined data while, θ refined result shows 8.397A°. The values show an increament of 0.041A°. and 0.001A° over 8.396A° obtained by Basta and O'Reilly (1967) for magnetite.

Although, the lattice constant obtained for the natural and synthetic samples in this work were generally slightly higher than those obtained by Rooksby

(1957) and Basta and O'Reilly (1967). This is due to the presence of impurities in the samples. The impurities can be attributed to some inadequacies of the various methods and mode of preparations of the synthetic samples.

However, other method, known as Crucible-less skull melting technique (Koenitzer et al, 1989) have been proposed and was used to grow 99.99% pure synthetic single crystal. Although, such technque can not be used presently within our own environment here due to lack of such equipment. However, the lattice constant values obtained from this work is still in agreement with the one obtained by Rigo et al, (1978). They have shown that the lattice constant of magnetite in presence of halogen range from 8.397A° to 8.428A°. This implies that the lattice constant of magnetite increases in the presence of an impurity which this work also confirmed.

4.3.0 Calculations of cell parameter by graphical method.

The computed values of the cell parameters described in section (4.2.1 to 4.2.5) were also compared with those obtained from the graphs in Fig. (4.7 - 4.12).

From Bragg's Law,

$2d \sin\theta = n\lambda$ ..... Eqn 4.2

for a cubic crystal $d = \frac{a}{(h^2+k^2+l^2)^{1/2}}$

$$\sin^2\theta = \frac{\lambda^2}{4a^2} Q^2, \quad Q^2 = (h^2+k^2+l^2) \qquad \text{..... Eqn 4.3}$$

From eqn 4.3 this shows that if a graph of $\sin^2\theta$ is plotted against Q^2 the graph should be a linear graph. From the slope, the value for the lattice parameter (a) can be obtained, with the X-ray wavelength known.

4.3.1 Natural sample: the X-ray diffracted angles of table 4.1 were plotted against the corresponding Miller Indices values. The value obtained for the lattice parameter from Fig. 4.7 was 8.621A°. When this value is compared with 8.403A° the lattice parameter obtained with the computer programme of appendix (A1) for the same set of θ values, it shows an increase of about 2.5% when compared with 8.396A° the value obtained by Basta and O'Reilly (1967) it shows an increase of about 2.7%.

4.3.2. Haber's method: From table 4.2, the square of the sine of diffracted angles were plotted against corresponding Miller indices, the value of lattice parameter obtained from the graph in Fig. 4.8 was 8.432A°. While, the computed value for the same set of θ values was 8.451A°. This shows that the graphical value is about 0.2% less than computed value.

4.3.3. Baudisch/Welo method: The graph of fig. 4.9 was obtained from the diffracted angles of table 4.3. The lattice constant obtained from the graph was

8.425A° while, the computed value was 8.443A°. Which implies that the graphical value is about 0.2% less than the computed lattice constant for this sample.

4.3.4 Elmore sample: The variation of the diffracted angles and the Miller indices was shown in Fig. 4.11 which was obtained from table 4.5. The lattice parameter obtained from the graph was 8.419A° while, the lattice costant computed for the same set of data was 8.411A°. For this sample, the two values obtained are almost the same.

4.3.5 Lefort sample: Fig. 4.10 shows the relationship between the diffracted angles and their corresponding Miller indices. The plotted values were obtained from table 4.4 the computed lattice constant was 8.438A° while, the graphical value was 8.465A° this implies that the graphical value of the lattice constant is 0.3% higher than the computed lattice constant value.

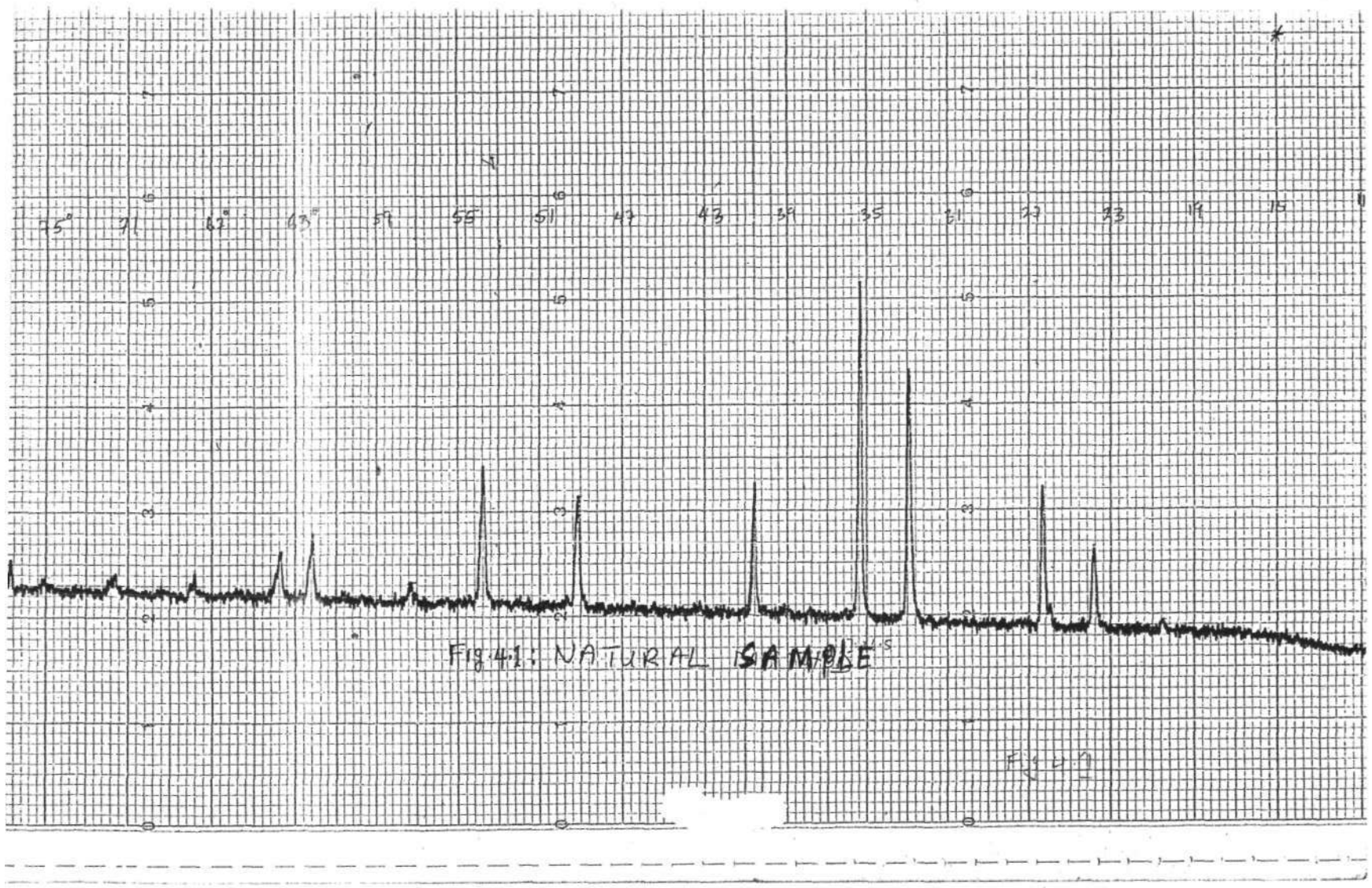


FIG 4.1: NATURAL SAMPLE



Fig 4.1: HAGER METHOD

Fig 4.2

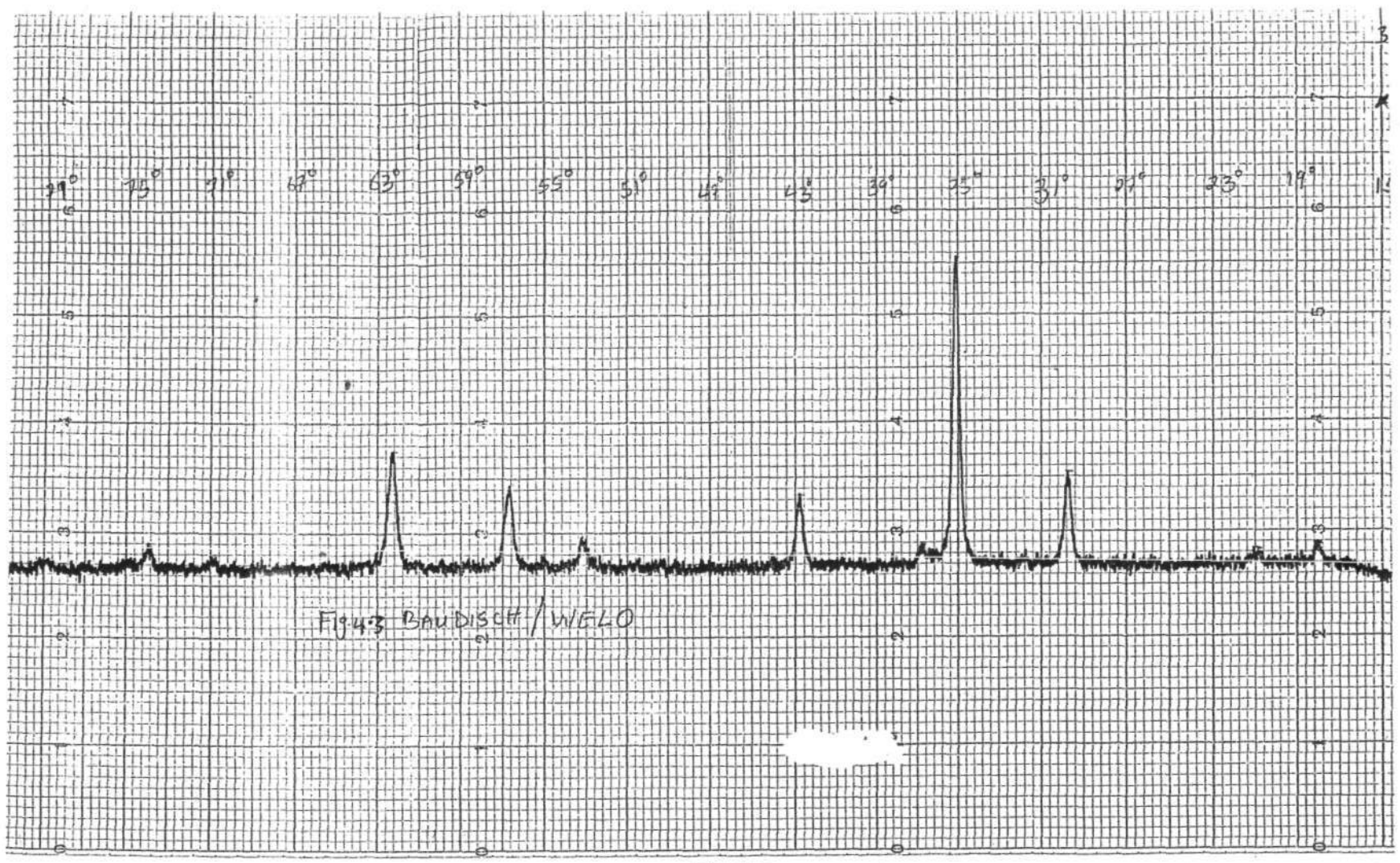


Fig 4.3

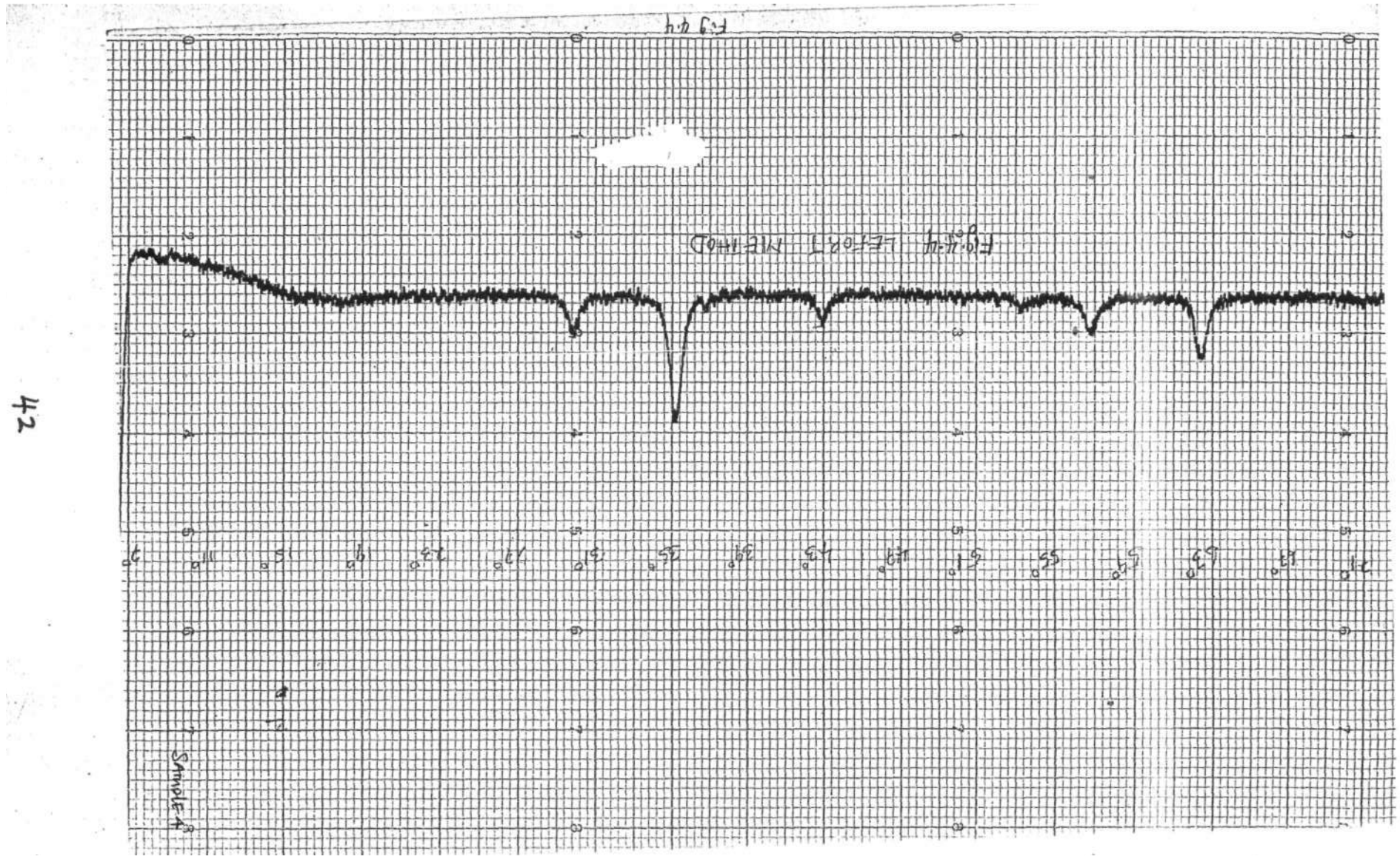
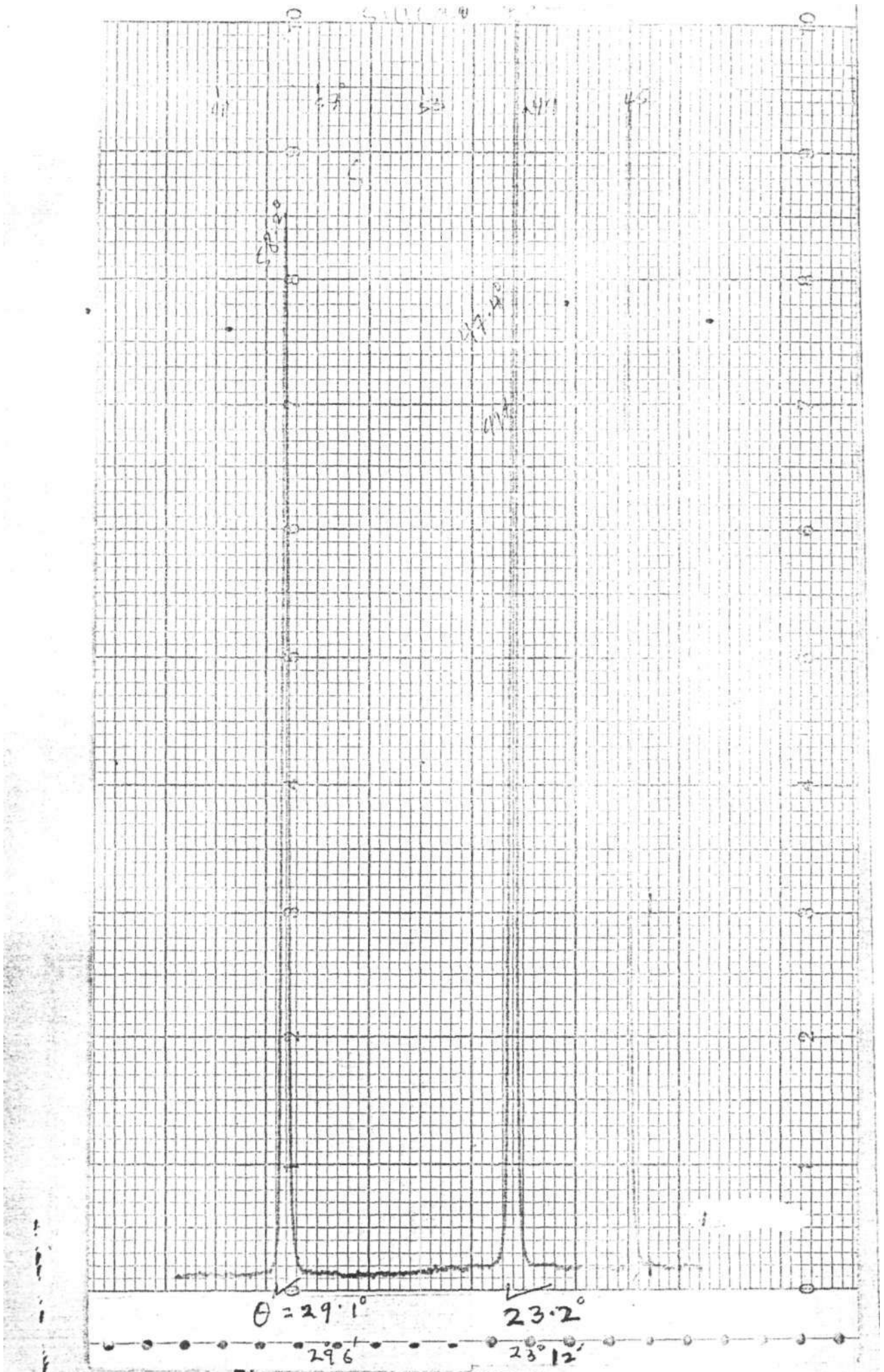

Fig 4.4
Experimental Laboratory Manual
Sample A



FIG 4.5 ELMORE METHOD

Fig 4.5



Fig·4·6: SILICA PEAKS.

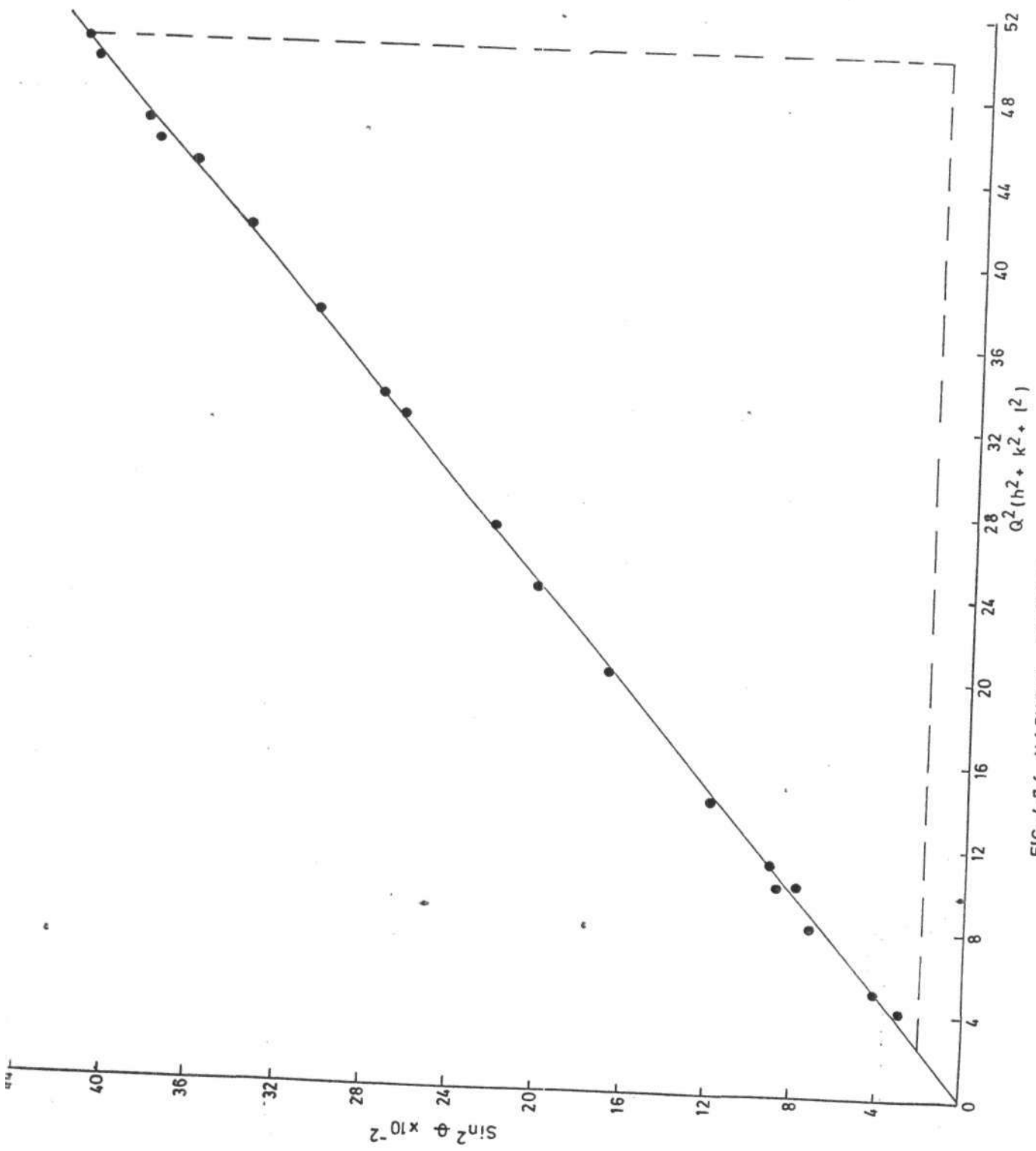


FIG. 4.7 : NATURAL SAMPLE

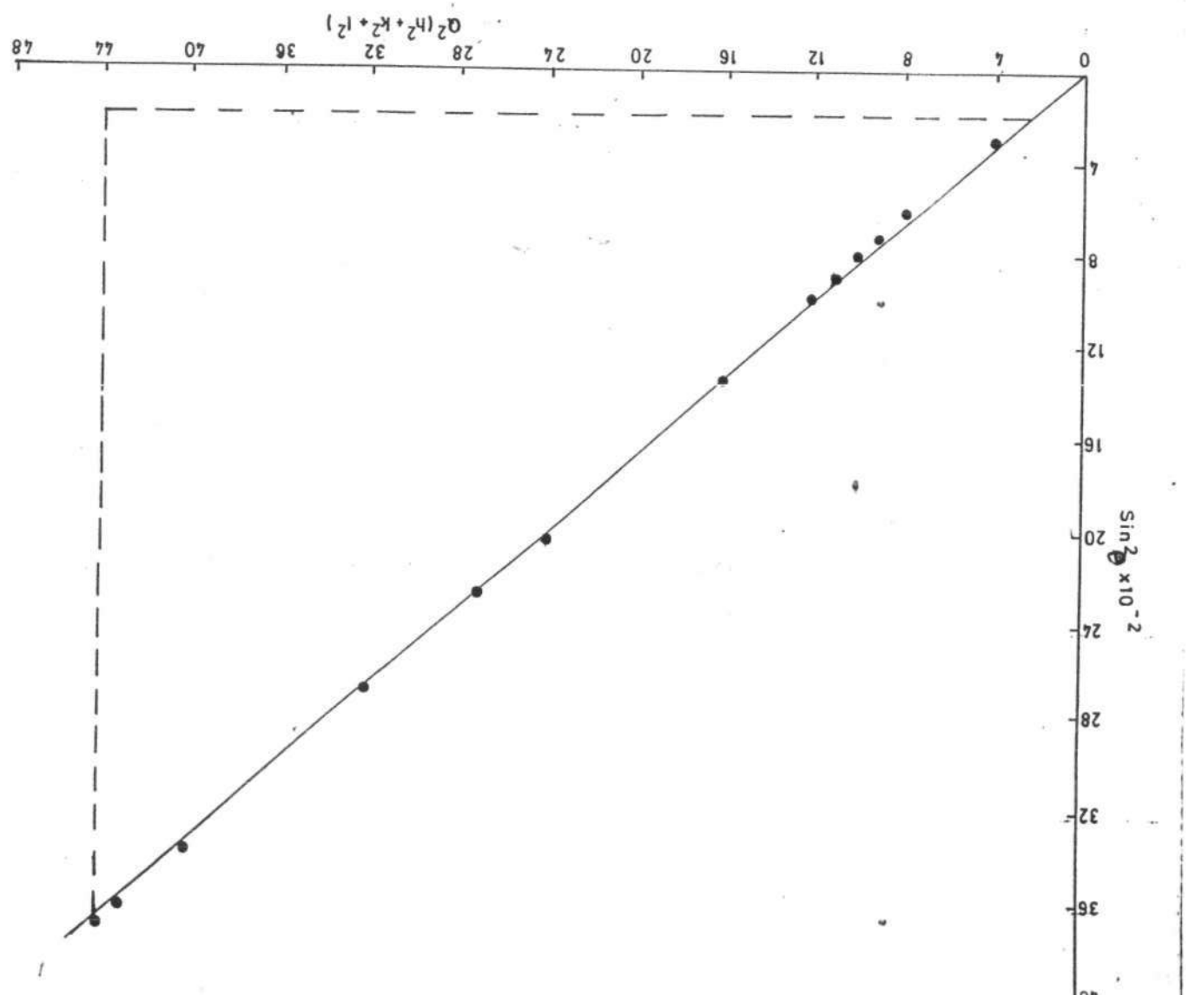


FIG. 4.8 : HABER'S METHOD

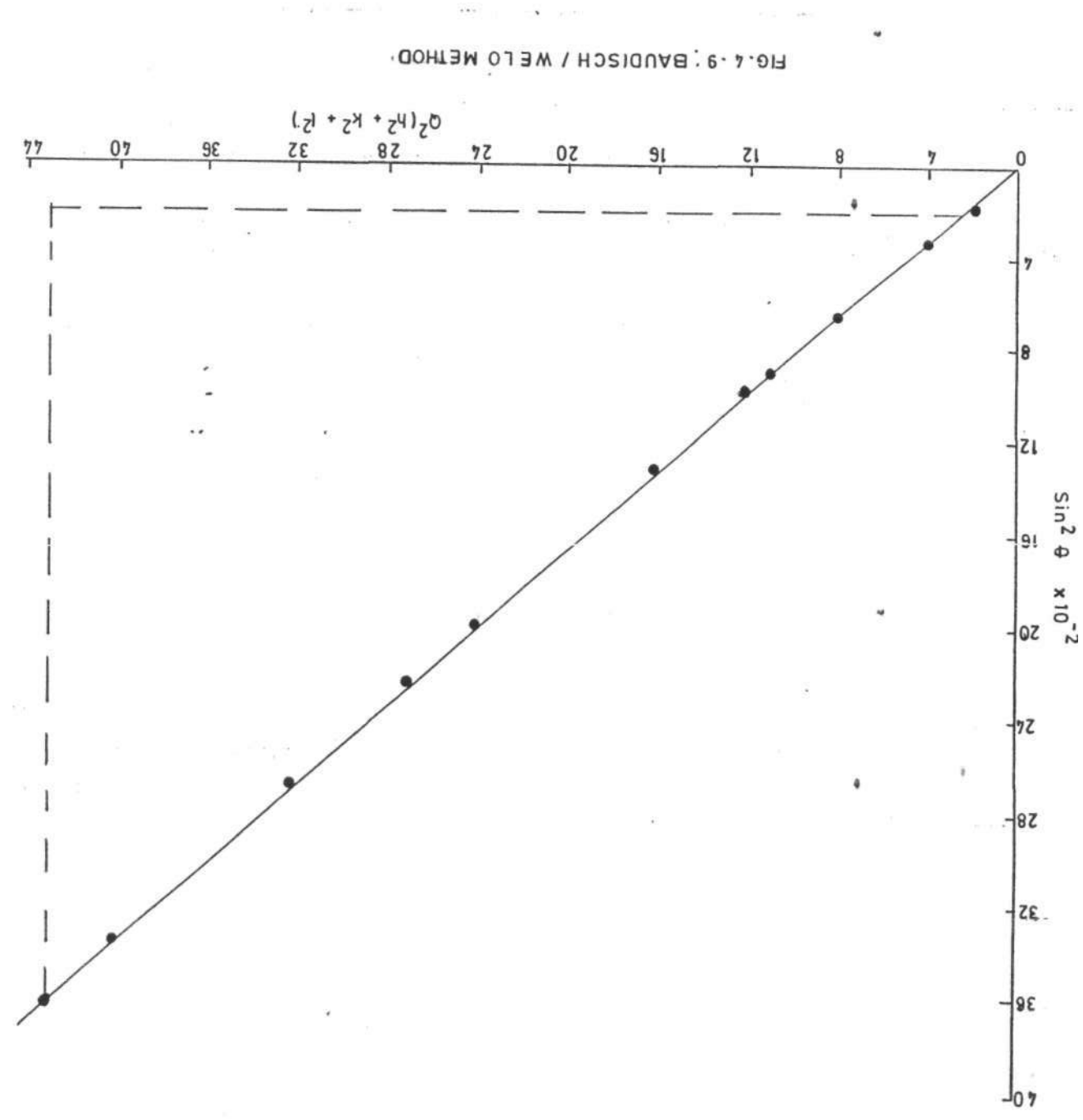


FIG.4.9 : BAUDISCH / WELO METHOD

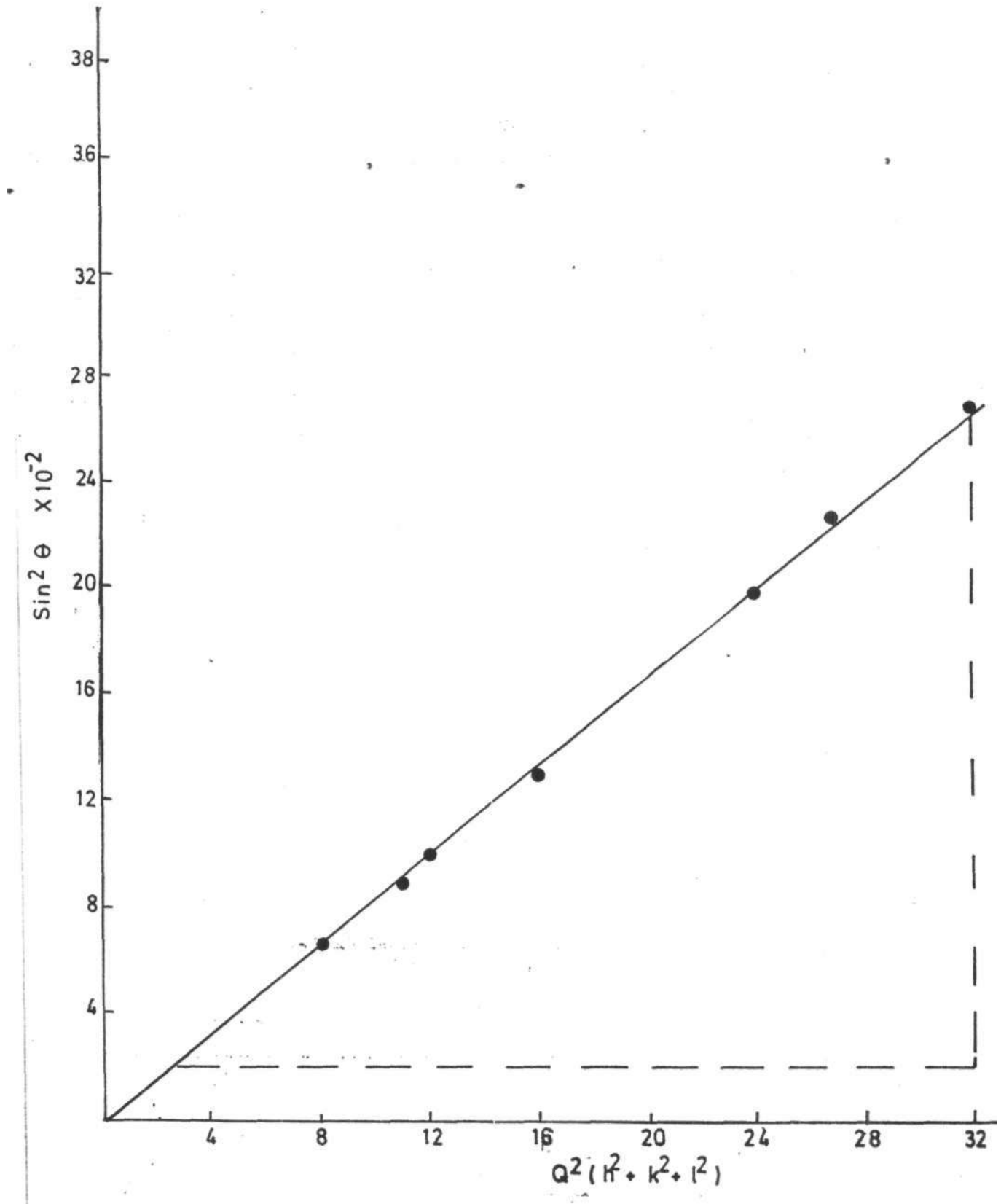


FIG. 4.10 : LEFORT SAMPLE

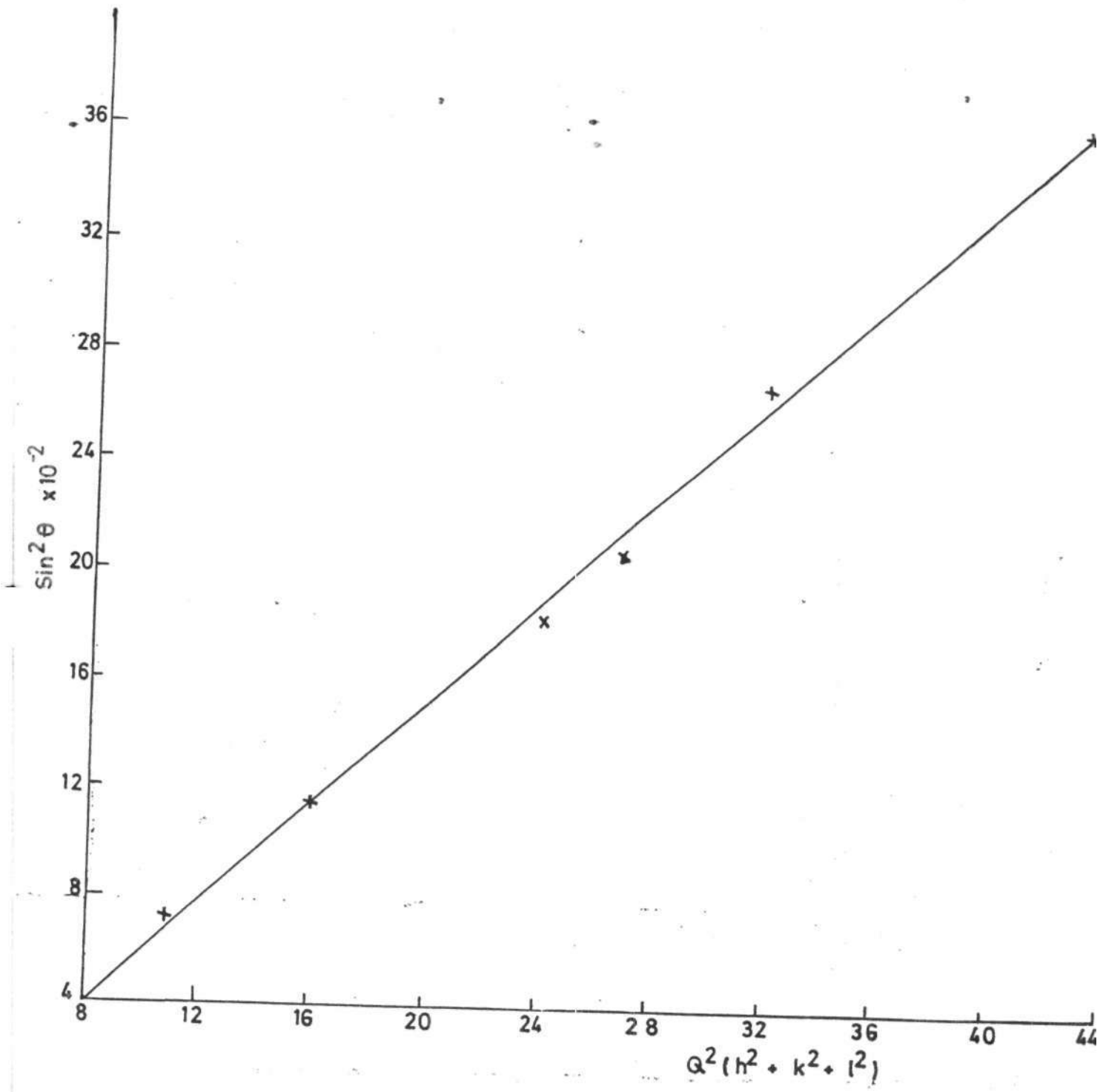


FIG.4.11: ELMORE METHOD

Table 4.1 - 4.5 Unrefined ● values

Table 4.1: Natural sample

Q° (Bragg angle)	Interplannar spacing d(A)	Relative Intensity I/I_ox00%	Miller indices (hkl)
10.20	4.3533	12	(200)
11.95	3.7231	32	(210)
13.20	3.3759	47	(220)
16.50	2.7143	77	(310)
17.70	2.5356	100	(311)
20.30	2.2220	48	(321)
24.55	1.8554	45	(420)
26.90	1.7029	52	(422)
28.65	1.6078	22	(511)(333)
31.10	1.4924	36	(440)
31.85	1.4609	30	(441)
33.90	1.3822	25	(610)
35.80	1.3179	25	(621)
37.50	1.2663	25	(622)
38.35	1.2424	28	(630(542)
38.60	1.2356	29	(631)
40.15	1.1956	27	(700)
40.40	1.1894	26	(710)(550)
Table 4.2	Haber's method		
10.00	4.4394	8	(200)
15.00	2.9785	29	(220)
16.90	2.6518	6	(310)

17.60	2.5495	100	(311)
18.40	2.4423	5	(222)
21.50	2.1034	25	(400)
26.70	1.7157	11	(422)
28.40	1.5704	29	(511)(333)
31.20	1.4881	39	(440)
35.40	1.3308	6	(620)
37.60	1.2809	10	(533)
37.50	1.2678	6	(622)
39.50	1.2119	6	(444)

Table 4.3 Baudisch/Welo

7.50	5.9061	13	(110)
10.40	4.2705	13	(200)
14.90	2.9981	34	(220)
17.55	2.5565	100	(311)
18.40	2.4423	13	(222)
21.40	2.1128	28	(400)
26.60	1.7312	16	(422)
28.30	1.6261	31	(511)(333)
31.15	1.4903	41	(440)
35.50	1.3275	10	(620)
37.00	1.2809	13	(533)

Table 4.4 Lefort's Method

14.90	2.9981	37	(220)
17.55	2.5565	100	(311)
18.40	2.4423	21	(222)
21.50	2.1034	36	(400)

26.60	1.7217	21	(422)
28.40	1.6208	39	(511)(333)
31.20	1.4881	53	(440)
37.00	1.2809	21	(533)

Table 4.5 Elmore's method

15.00	2.9785	43	(220)
17.60	2.5495	100	(311)
21.50	2.1034	35	(400)
26.8	1.7098	19	(422)
28.5	1.6156	35	(511)(333)
31.3	1.4839	54	(440)
37.1	1.2780	17	(533)

Table 4.6 - 4.10 refined θ values with silica.

Table 4.6: Natural sample

θ° Bragg angle(θ)	Interplanner spacing d(Å)	Relative Intensity $I/I_o \times 100\%$	Miller indices (hkl)
9.16	9.6124	12	(111)
10.46	8.4250	32	(200)
12.16	7.2546	47	(012)
15.46	5.7167	77	(220)
16.66	5.3085	100	(310)
19.26	4.5988	48	(320)
23.51	3.7856	45	(331)
25.66	3.4663	52	
27.61	3.2318	22	(340)(500)
30.06	2.9688	36	(251)

30.81	2.9030	30	
32.86	2.7223	25	(351)
34.76	2.5779	25	
36.46	2.4616	25	(451)
37.31	2.4107	28	(226)
37.56	2.3921	29	(622)
39.11	2.3037	27	
39.36	2.2758	26	(444)

Table 4.7 Haber's method

8.96	9.8255	8	(111)
13.96	6.3256	29	
15.86	5.5738	6	(122)
16.56	5.3403	100	(310)
17.36	5.0965	6	(311)
20.46	4.3323	25	(321)
25.66	3.4663	11	(332)
26.96	3.3023	29	(422)
30.16	2.9592	39	(521)
34.36	2.6070	6	(532)(611)
35.96	2.4947	10	(045)(621) (443)
36.46	2.4616	6	(451)
38.46	2.3382	6	(631)

Table 4.8 Baudisch/Welo method

Bragg angle(θ)°	Interplanner spacing d(A°)	Relative Intensity I/I_ox100%	Miller indices (hkl)
6.46	13.5979	13	(110)
9.36	9.4083	13	(111)
13.86	6.3709	34	
16.51	5.3724	100	(310)
17.36	5.0965	13	(311)
20.36	4.3533	28	(321)
25.56	3.4796	16	(332)
27.26	3.2666	31	(500)(430)
30.16	2.9592	41	(521)
34.46	2.5996	10	
35.96	2.4947	12	(540)(621) (443)

Table 4.9 Lefort's Method

13.86	6.3709	37	
16.51	5.3724	100	(310)
17.36	5.0965	21	(311)
20.46	4.3323	36	(321)
25.56	3.4796	21	(332)
27.36	3.2550	39	(500)(430)
30.16	2.9592	53	(521)
35.96	2.4942	21	(540)(443)

Table 4.10 Elmore's method

13.96	6.3256	43	
16.56	5.3403	100	(310)

20.46	4.3323	35	(321)
25.76	3.4531	19	(233)
27.46	3.2433	35	(500)(430)
30.26	2.9497	54	(521)
36.06	2.4947	17	(621)(443)

4.4.0 **ENERGY DISPERSIVE X-RAY FLUORESCENCE RESULT**

The impurities as well as their concentration associated with the natural and synthetic samples were determined. The concentration of each of the elements present in each sample was calculated by using the formula

$$C = \frac{I_n}{g_o \times k_i \times \rho d_i} \qquad \text{Eqn 4.1}$$

C = Concentration

I_n = Net intensity

g_o = Geometrical factor of cadmium source (233215.956)

k_i = K. transition line value

ρd_i = mass per unit area.

The summary of the result is shown in table 4.6 to 4.10.

4.4.1 Natural Sample: Table 4.6 shows the various elements presents in the sample as well as their concentrations the results, show that the major impurities in this sample are chlorine (Cl) Calcium (Ca). While elements like Copper, Zinc and Lead are

present in the form of trace elements. The percentage of iron concentration is 34% which is quite low when compared to other synthetic samples.

4.4.2 Haber's method: The impurities present in this sample were shown in table 4.7. Among the elements present in the sample as impurities, chlorine has the highest percentage of 1.35%, followed by calcium and pottasium. Others impurities present as minor elements are strontium and yitterbium and lead. However, the concentration of iron is 70.4%. This is more than twice the iron concentration in the natural magnetite.

4.4.3 The method of Baudisch and Welo: Table 4.8 shows the elements present in the sample as well as their concentrations. This sample gave the least number of impurities. The major impurities are chlorine, potasium and calcium other trace impurities are: Strontium, yitterbium and Zinc. However, the percentage of iron concentration in the sample is 70% the same concentration as that of Haber's method.

4.4.4 Elmore's method: The impurities present in this sample as well as their concentration is shown in table 4.9. The major impurities are chlorine and lantanium. While trace elements are yitterbium, strontium and Nickel. The iron concentration in this sample is 76% which is higher than those concentrations obtained for previous samples.

4.4.5 Lefort's method: Table 4.10 shows the summary of the elements present in this sample as well as their concentrations. This sample has the largest number of impurity elements. Most of which may be present in the oxides and various container used during the preparation of the sample. The major impurities are: chlorine, manganesse and lantanium while, the trace elements includes yitterbium, Zinc and strontium.

The iron concentration in this sample was found to be 78%. This shows that it has the largest concentration of iron when compared to other samples like Haber, Elmore and Natural samples.

RESULTS OF THE IMPURITIES PRESENT IN THE SAMPLES

NATURAL SAMPLE Table 4.11

Element	Net Intensity (I_n)	Ki (values	Mass Per Unit area	Concentration $C=I_n/g_o k_i \rho d_i$	% concentration
CL	0.159330	0.169510	5.7098×10^{-4}	0.0070586	0.70586
K	0.055189	0.53203	5.7098×10^{-4}	0.0007789	0.07789
Ca	0.806620	0.83259	"	0.007275	0.72750
Ti	0.197539	1.550350	"	0.0009568	0.09568
Fe	202.4070	4.44992	"	0.34158	34.158
Cu	0.079948	7.76950	"	0.0000772	0.00772
Zn	0.103855	9.25407	"	0.0000842	0.00842
Sr	0.424157	22.7009	"	0.0001403	0.01403
Y	0.461487	24.9850	"	0.0001387	0.01387
Pb	0.022996	7.8800	"	0.0000219	0.00219

Haber's Method Table 4.12					
CL	0.301667	0.169510	5.66154×10^{-4}	0.0134784	1.34784
K	0.290245	0.53203	"	0.0041317	0.41317
Ca	0.809460	0.83259	"	0.007363	0.7363
Fe	413560	4.44992	"	0.7030716	70.3872
Cu	0.03947	7.7695	"	0.0000384	0.00384
Sr	0.0034315	22.7009	"	0.0000011	0.00011
Y	0.066181	24.9850	"	0.00002	0.00200
Zr	0.088548	27.2166	"	0.0000246	0.00246
Ba	0.0178306	0.5477	"	0.0002465	0.00246
Pb	0.030671	7.8800	"	0.000029$	0.00294
Baudish and Welo Table 4.13					
CL	0.104791	0.16951	5.46645×10^{-4}	0.004902	0.49029
K	0.244805	0.53203	"	0.0036493	0.3649
Ca	0.75849	0.83259	"	0.0072251	0.72251
Fe	393.160	4.4499	"	0.7007235	70.072
Sr	0.009684	22.7009	"	0.000033	0.00033
Y	0.031662	24.985	"	0.000010	0.001
Nb	0.053278	29.5843	"	0.0000142	0.00142
Elmore method 4.14					
CL	0.18979	0.16951	3.680×10^{-4}	0.0130463	1.30463
K	0.000733	0.53203	"	0.000016	0.0016
Mn	0.62587	3.46497	"	0.0021046	0.21046
Fe	296.600	4.44992	"	0.7681212	76.81212
Ni	0.02957	6.82268	"	0.0000505	0.00505
Cu	0.05221	2.76950	"	0.0000783	0.00783
Zn	0.16064	9.25407	"	0.0002022	0.02022

Zr	0.021901	22.7009	"	0.0000112	0.00112
Y	0.05342	24.9850	"	0.0000249	0.00249
La	0.66376	0.64120	"	0.0121093	1.21093
Pb	0.090634	7.8800	"	0.000134	0.0134
Lefort method Table 4.15					
CL	0.165697	0.16951	2.76129×10^{-4}	0.0151792	1.51792
K	0.030214	0.53203	"	0.0008818	0.08818
Ca	0.54532	0.83259	"	0.001017	0.1017
Ti	0.0451996	1.55035	"	0.0004527	0.04527
Cr	0.0674931	2.76471	"	0.0003791	0.03791
Mn	0.7829098	3.46497	"	0.0035086	0.35086
Fe	222.423	4.44992	"	0.7761706	77.6170
Cu	0.050799	7.7695	"	0.0001015	0.01015
Zn	0.042154	9.25407	"	0.000707	0.00707
Sr	0.018470	22.7009	"	0.000126	0.00126
Y	0.304866	24.985	"	0.0001894	0.01894
Zr	0.033109	27.2166	"	0.0000188	0.00188
La	0.377709	0.6412	"	0.0091473	0.91473
Pb	0.083644	7.880	"	0.0016483	0.16483
Th	0.02295	10.3128	"	0.0000345	0.00345

Table 4.17 - 4.21: Bragg angle (θ) with polarization-factor values

Table 4.17: Natural sample

θ (refined) Bragg angle(θ)	Lorentz-Polarization factor $[1+\cos^2\theta/\sin^2\theta\cos\theta]$
9.16	75.31
10.46	57.32
12.16	41.91
15.46	25.21
16.66	21.46
19.26	15.62
23.51	10.05
25.66	8.20
27.61	6.97
30.06	5.73
30.81	5.45
32.86	4.72
34.76	4.19
36.46	3.82
37.31	3.17
37.56	3.61
39.11	3.38
39.36	3.33

Table 4.18 Haber's method

8.96	78.79
13.96	31.34
15.86	23.86

16.56	21.74
17.36	19.62
20.46	13.66
25.66	8.20
26.96	7.33
30.16	5.69
34.36	4.29
35.96	2.92
36.46	3.82
38.46	3.47

Table 4.19 Baudisch/Welo method

6.46	153.10
9.36	72.05
13.86	31.82
16.51	22.02
17.36	19.62
20.36	13.81
25.56	8.27
27.26	7.15
30.16	5.69
34.46	4.27
35.96	3.92

Table 4.20 Lefort sample

13.86	31.82
16.51	22.02
17.36	17.62
20.46	13.66
25.56	8.27

27.36	5.69
30.16	5.69
35.96	3.92

Table 4.21 Elmore' sample

13.96	31.34
16.56	21.94
20.46	13.66
25.76	8.13
27.46	7.03
30.26	5.65
36.06	3.90

4.5.0 Possible errors in the relative intensity of the diffraction pattern.

The possible errors in relative intensities shown in Fig. (4.1 - 4.6) is hereby discussed: There are six factors affecting the relative intensity of the diffraction pattern of a powder sample.

a) Polarization factor

b) Structure factor

c) Multiplicity factor

d) Lorentz Factor

e) Absorption factor

f) Temperature factor

The two most prominent factors which affect the relative intensity are the lorentz and polarization factors.

Lortentz factor: If all the diffracted beams sent

out by the powder sample as it rotates through the Bragg angle (θ) are received in a counter, the total energy of the diffracted beam can be measured. This energy is called 'the integrated intensity of the' reflection and is given by the area under the diffraction peak. The integrated intensity of a reflection depends on the particular value of Bragg angle (θ) involved even though all other variables are kept constant. Thus, as a crystal is rotated through the Bragg angle, the integrated intensity of a reflection, which is the quantity of most experimental interest, turns out to be greater for large and small values of 2θ values than for intermediate values, other variables being constant.

In intensity calculations, the factors discussed are combined into one factor called lorentz-polarization factor.

$$\text{Lorentz-Polarization factor} = \frac{1 + \text{Cos}^2 2\theta}{\text{Sin}^2\theta\text{Cos}\theta}$$

θ = Bragg angle

Tables 4.17 - 4.21 shows the Bragg angle and the corresponding polarization factor values. While, Fig. (4.12 - 4.16) shows the Bragg angle variation with polarization factor for each of the sample

Generally, from the curves (Fig. 4.12 - 4.16). It can be concluded that the over-all effect of these geometrical factors is to decrease the intensity of reflections at intermediate Bragg angles ($0<\theta<45^{\circ}$).

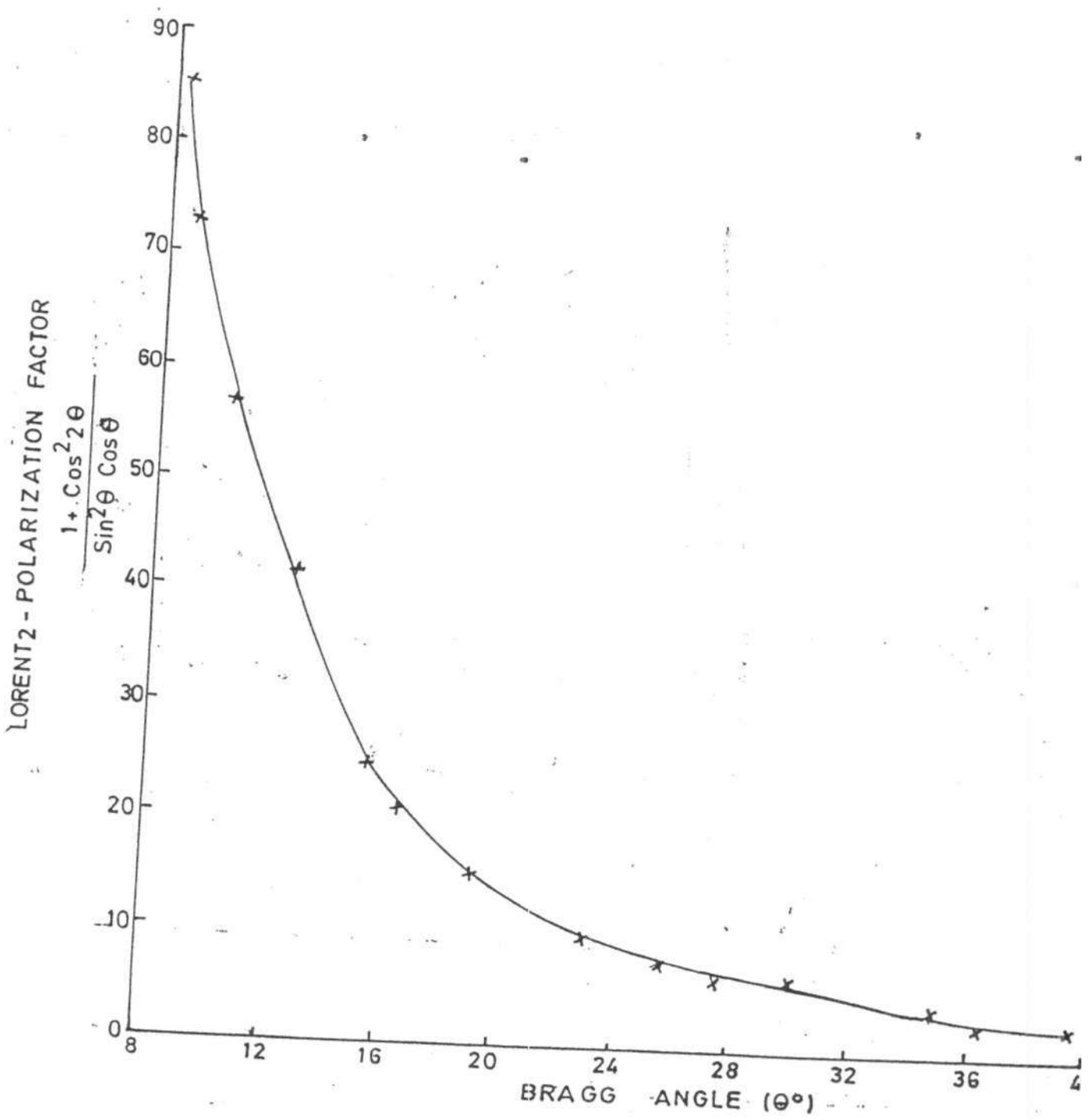


FIG. 4.12 : NATURAL SAMPLE

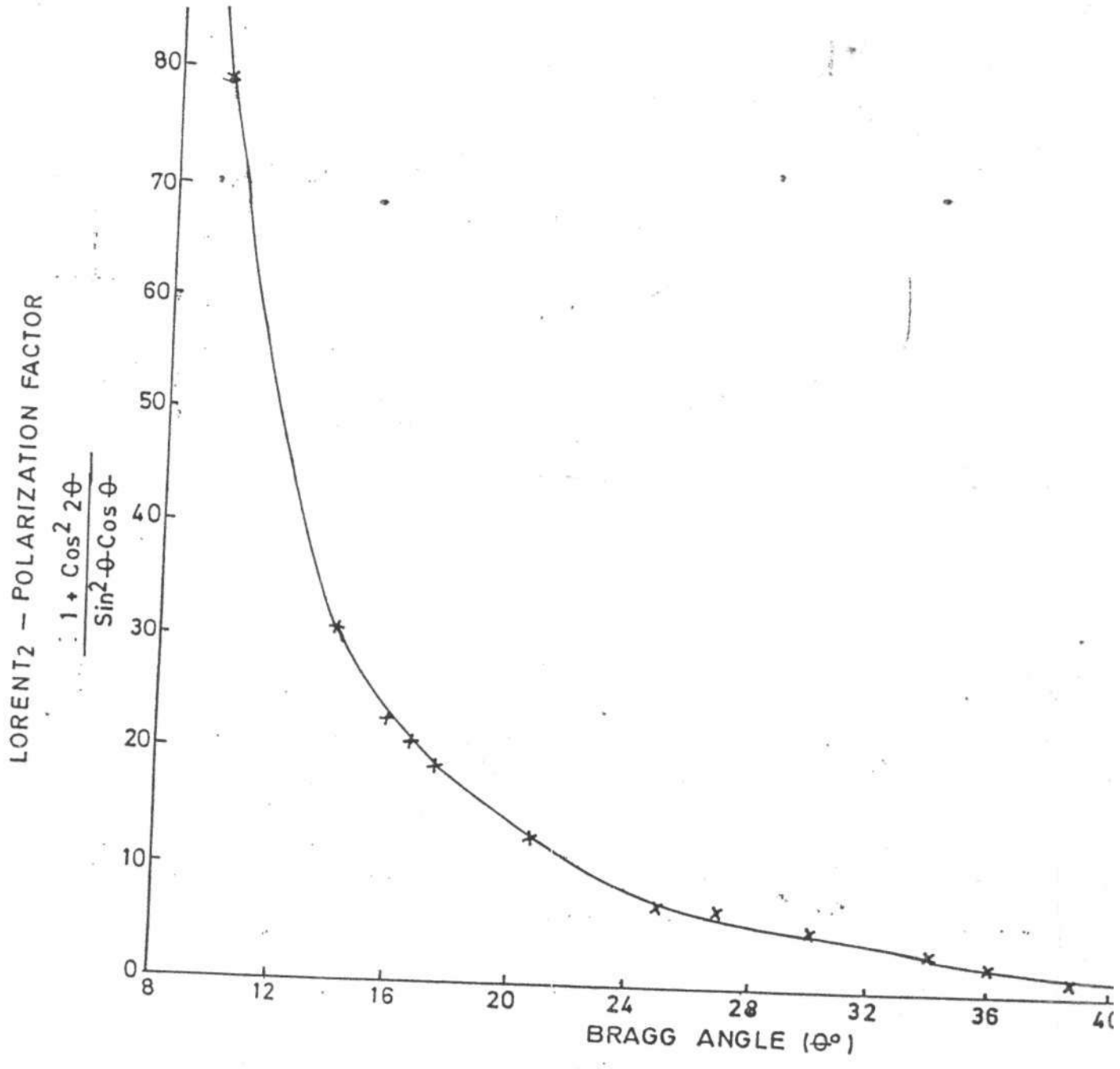


FIG. 4.13 : HABER : SAMPLE

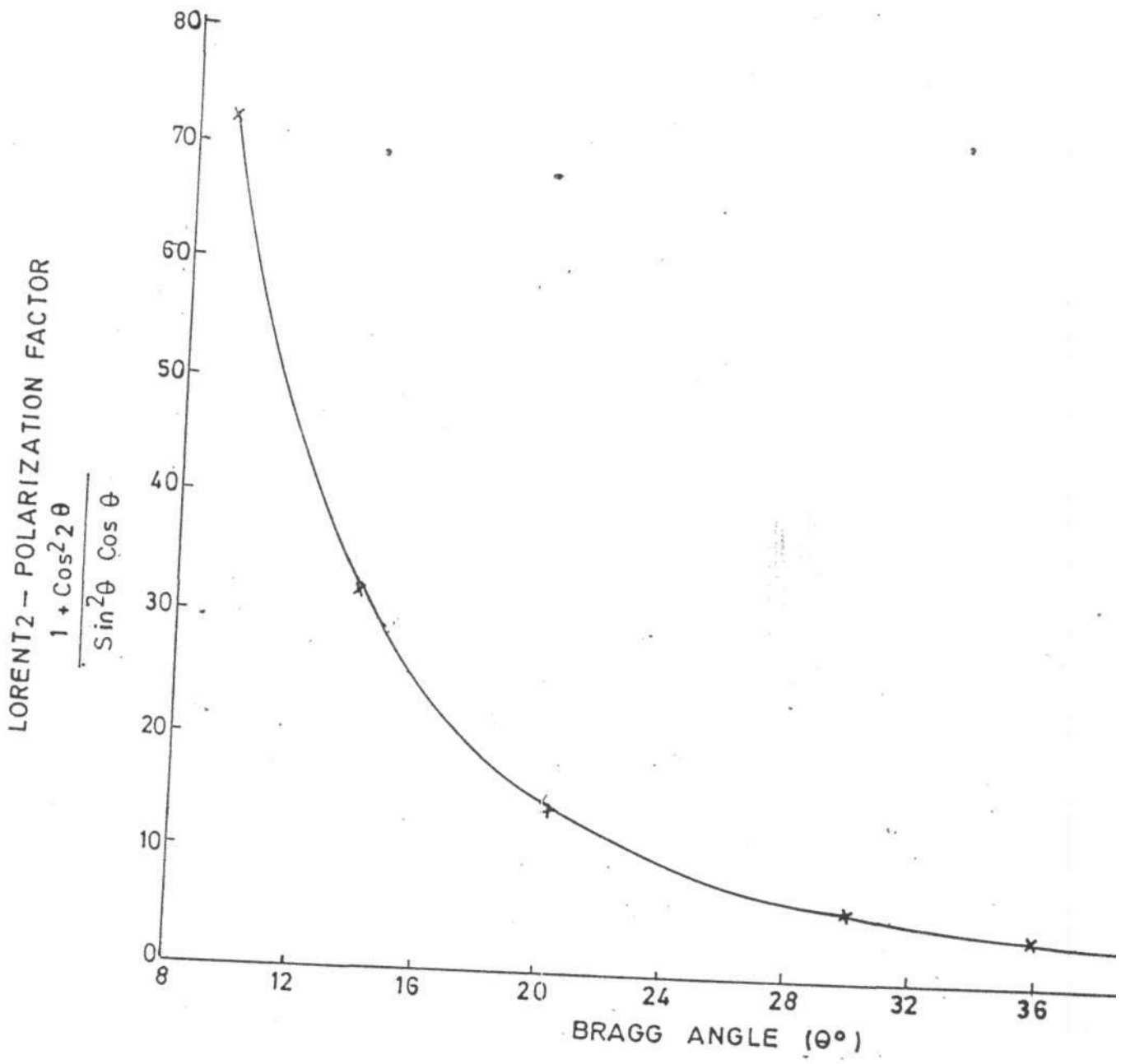


FIG. 4.14 : BAUDISCH / WELO SAMPLE

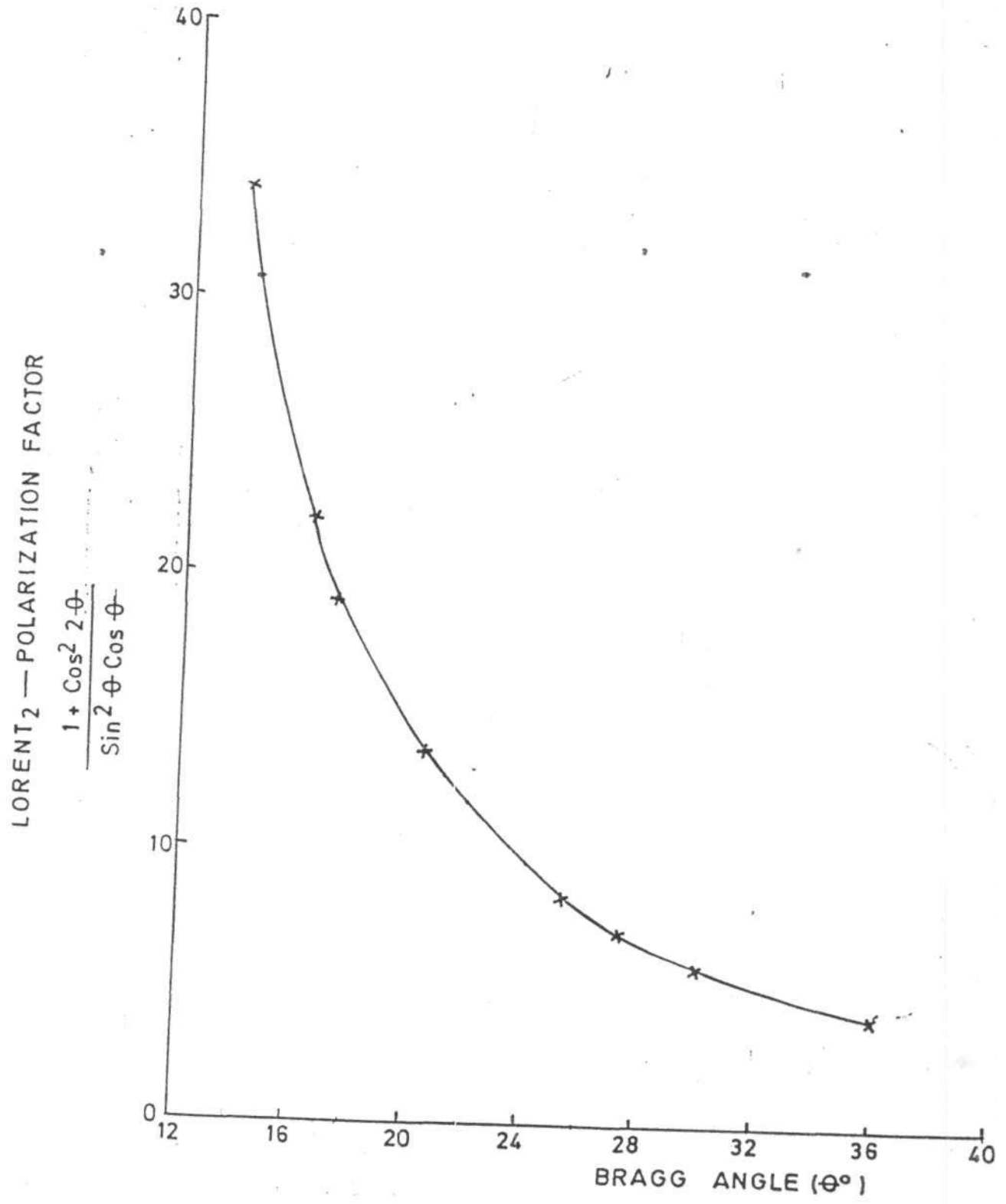


FIG-4.15 : LEFORT. SAMPLE

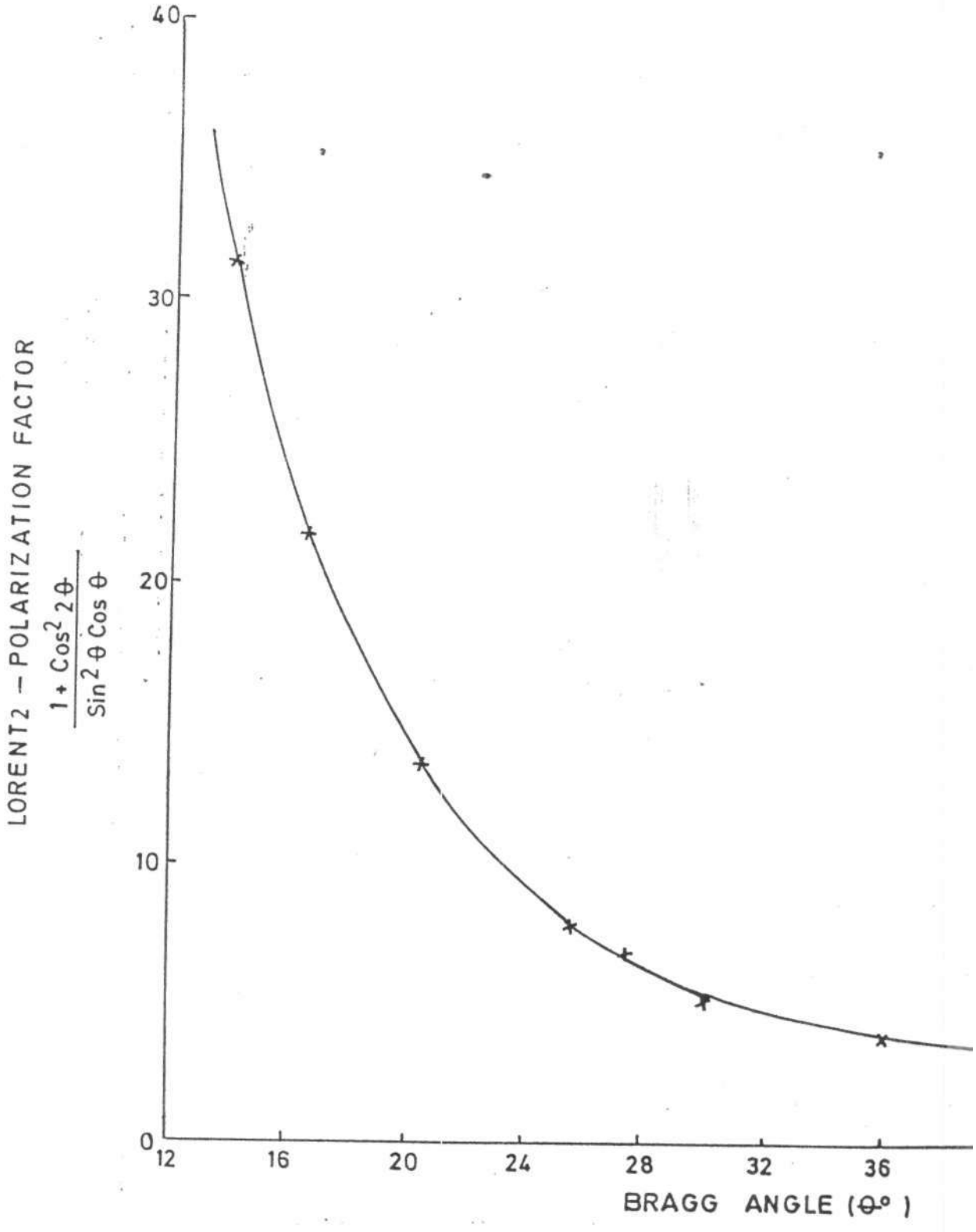


FIG.4.16: ELMORE SAMPLE

Table 4.16 Summary of Lattice Parameter values.

Sample	Lattice constant θ refined (A^o)	Lattice constant θ unrefined (A^o)	value of latt. obtained by other workers.		
Natural	8.398	8.403	Rooksby	8.394	Pure Fe_3O_4
Haber	8.426	8.451	Basta	8.396	" "
Baudisch/ Welo	8.411	8.443	O'Reilly	8.396	" "
Elmore	8.397	8.411	Rigo, et al	8.397	in the presence of halogen
Lef ort	8.423	8.438		8.4238	

4.6.0 Limitations and suggestions for future works

There are some limitations and possible sources of error which this work have not been able to eliminate completely, for example, the choice of the methods used for the preparation of the synthetic samples do not guarantee 99% pure sample when one compare the methods used in this work to modern methods such as skull-melting technique (Koenitzer et al, 1989) and hydrothermal growth (Gilman, 1963) of preparing pure magnetite.

Although, the diffracted angle θ obtained in this work were refined using the silica standard peaks Fig. 4.6. other forms of errors described earlier in sections 2.5.0 to 2.5.5 should have also been corrected for. Also, it would have been better if Cobalt target was used during the analysis of the samples instead of

using copper target because cobalt radiation is normally used for iron associated X-ray analysis in order to prevent high background that results from the fluoresence of iron by copper radiation.

CHAPTER V

CONCLUSIONS

In this report, comparative studies of both synthetic and natural magnetite has been carried out. The synthetic samples were prepared by the methods proposed by Lefort, Elmore, Baudisch/Welo and Haber. The natural sample which the results of the synthetic samples were compared, was obtained from iron-ore deposits at Itakpe-Okene in Kogi state.

The XRD was used to determine the cell parameter for each of the samples while, EDXRF was used to determined the impurities present in each sample and their concentration. The lattice parameter of the natural magnetite was found to be 8.398A^{o} while, the percentage concentrations of iron was 34%. The lattice parameter calculated for Haber method was 8.426A^{o} while, the concentration of iron in the sample was determined to be 70.4%. The cell parameter obtained for Baudisch/Welo method was 8.411A^{o}. The EDXRF result gave the concentration of iron in this sample as 70%. The XRD analysis show that the cell parameter for lefort sample was 8.423A^{o} while the EDXRF result gave the iron concentration in the sample as 78%. This implies that this sample has the highest concentration of iron in it. The XRD analysis of the Elmore method shows that the lattice constant for this sample was 8.397A^{o} while EDXRF result gave the concentration of iron to be 76%.

Although, if the values obtained for the lattice parameters for the five samples were compared with 8.396A° obtained for pure magnetite by Basta (1957) and O'Reilly (1967) there is a slight increase between (0.007A° - 0.044A°) in the results obtained in this work. This increase in the cell parameter is due to the presence of impurities in the lattice of both the synthetic and natural sample.

However, the lattice parameters obtained for the natural and synthetic samples were in agreement with the result obtained by Rigo et al, (1978). They have shown that the lattice parameter of magnetite in the presence of halogen impurity range from 8.397A° to 8.428A°.

REFERENCES

Aragon, R. et al, (1986) Journal of Mag. And Mag. Mat. 1335

A.I.P. Con. Proc. (1974) No. 24, p. 73

A.I.P. Con Proc. (1976) No. 34, p. 181

Bartel J.J. and Westrum E. Jr. (1974) A.I.P. Conf. Proc. 18, 1393 (1974)

Basta, E.Z, (1957) Miner, Mag. 31, 431

Bickford, Jr. L.R., (1950) Phy. Rev. 78, 4, 449

Bond, W.L., (1959) Acta Cryst. 13, 814 .

Bragg, W.L., (1915) Phil. Mag. 30 p. 305 .

Calhoun, B.A., (1954) Phys. Rev. 94, 1957

Cullen, J. R. and Callen E. (1970), J. Apl. Phys. 41, 879.

Compton, A.H. and Allison, S.K. (1935). X-rays in Theory and Experiment. London Macmillan.

Elmore, W.C., (1938) Phys. Rev. 54, 309

Evans, B.J. and Westrum, E.F. (1972) Phys. Rev. B5 3791

Freidrich, W, Knipping, P., Von Laue (1912) Akad. Wiss 303.

Gibbons, D. (1958). Phys. Rev. 112, 137.

Hamilton W.C. (1958) Phys. Rev. 110, 1050.

Koenitzer, J.W., et al, (1989) Phy. Rev. B, 39, 9, 6231 .

Kuipers and Brabers, (1977) Phys. Rev. Lett. 39, (8) 488

Li, C.H., (1932) Phys. Rev. 40, 1002

Mills et al, R.E. (1966) Phys. Rev. 145, 704

Mott, N.F., (1969) Phil. Mag. 20, 163 .

O'Reilly Acta. Cryst. (1968) B24, 422

Okamura, Science reports, (1932). Tohoku Imp. Univ. 13,21,231

Orlic, I, et al, (1988) X-ray spectrometry, 17, 139-143

Rigo, M.O., et al., (1978) Solid state commun. 28, 1013

Richtmeyer, F.K. (1947). Introduction to Modern Physics. New York. Mcgraw-Hill.

Roetgen, W.C. (1898) Ann. Phys. Chem. 64, 1.

Rooksby, H.P., (1961) London Miner. Society

Shapiro, L.M., (1976) Phys. Rev. B14(1), 200

Shepherd, J.P., et al, (1985) Phys. Rev. B, 32, 3, 1818 .

Shull et al, (1951) Phys. Rev. 912

Sokoloff, (1972) Phys. Rev. B5, 4496

Verwey, E.J., (1939) Nature 144, 327

Verwey E.J. and Haayman, (1941). Physica 8, 879.

Welo L.A. and O Baudisch, (1927) Phil. Mag 3, 396 .

Yamada, T et al, (1968) Appl. Phys. Lett. 13, 172,

APPENDIX A

```
PROGRAM XRD1;

USES DOS,CRT;

  CONST
    LAMBDA=1.5418E-10;
    TYPE
      ARRAYTYPE=ARRAY[1..20]OF REAL;
      VAR
      THETA,X,Q,C:ARRAYTYPE;
      THETAC,SUMC,SD,FACTOR,NUM,AVEC,AVALUE,SD_A:REAL;
      I,H,K,L,N:INTEGER;
      NATURAL,RESULT:STRING[79];
      INPUTFILE,OUTPUTFILE:TEXT;
     BEGIN
        CLRSCR;
        WRITE('ENTER A VALID INPUT FILE NAME : ');READLN(NATURAL);
        WRITE('ENTER A VALID OUTPUT FILE NAME : ');READLN(RESULT);
        SUMC:=0.0;
        NUM:=0;
      ASSIGN(INPUTFILE,NATURAL);
      RESET(INPUTFILE);
      N:=0;I:=0;
           WHILE NOT EOF(INPUTFILE) DO
           BEGIN
           I:=I+1;
           READLN(INPUTFILE,THETA[I],H,K,L);INC(N);
           THETAC:=THETA[I]*PI/180;
           X[I]:=SQR(SIN(THETAC));
           Q[I]:=SQRT(SQR(H)+SQR(K)+SQR(L));
C[I]:=X[I]/SQR(Q[I]);
SUMC:=SUMC+C[I];
END;
CLOSE(INPUTFILE);
ASSIGN(OUTPUTFILE,RESULT);
REWRITE(OUTPUTFILE);
 AVEC:=SUMC/N;
 AVALUE:=LAMBDA/(2*SQRT(AVEC));
  FOR I:=1 TO N DO
    NUM:=NUM+SQR(AVEC-C[I]);
  IF N>10 THEN SD:=SQRT(NUM/(N-1)) ELSE SD:=SQRT(NUM/N);
SD_A:=LAMBDA/(2*SQRT(SD));
WRITELN(OUTPUTFILE);
WRITELN(OUTPUTFILE,'A-VALUE AND ITS STANDARD DEVIATION');
WRITELN(OUTPUTFILE,AVALUE,SD_A);
CLOSE(OUTPUTFILE);
WRITELN('.....DONE');READLN;
END.
```

```
program crystallography (indata,outdata,output);
  {this code calculates the d-spacing,qvalueand crystal planes for a giv
      angle theta}
uses dos,crt;
    const
         lambda=1.5418;
         a=8.396;
         pi=3.142;
    var
         outdata,indata,outdata1:text;
         datafilename,resultfilename,resultfilename1:string[79];
         vcround:integer;
         theta,
         dspacing,
         qvalue,
         radperdeg,
         radian,
         fact0,
         fact1,
         fact1num,
         fact1den,
         vc:real;

    function raisetopower(number:real;power:integer):real;
       {this function calculates the value of a number
        raise to power}

        begin{power}
          raisetopower:= exp(power*ln(number))

        end;{ power}

  procedure hkl(x:integer);

     {this procedure calculates the values of hkl for a
      specific angle i.e determines the crystal planes}

    var
        h,k,l,rootx,temp:integer;

    begin {hkl}
    write(outdata1,theta:5:2);
          rootx:=round(sqrt(x));
          for h:=0 to rootx do
           begin
            for k:=0 to rootx do
              begin
               for l:=0 to rootx do
                begin
                  temp:=sqr(h)+sqr(k)+sqr(l);
                  if temp=x then write(outdata1,' ',h,' ',k,' ',l,' ');
```

```
                end;
              end;
            end;
          writeln(outdata1);
    end;{hkl}

begin{main program}
clrscr;
write('Enter data file name : ');readln(datafilename);
resultfilename:= datafilename+'.res';
resultfilename1:=datafilename+'.re1';
assign(indata,datafilename);
assign(outdata,resultfilename);
assign(outdata1,resultfilename1);

     reset(indata);
     rewrite(outdata);
     rewrite(outdata1);
     writeln(outdata,'theta     radians     dspacing  qvalue',
             'fact0  factone  vc    hkl ');

      while not eof(indata) do
        begin
          readln(indata,theta);
          radperdeg:=pi/180;
          radian:=radperdeg*theta;
          dspacing:=lambda/(2*sin(radian));
          qvalue:=1.0/sqr(dspacing);
          fact0:=cos(radian)/sin(radian);
          fact1num:=raisetopower(lambda,4);
          fact1den:=sqr(sin(2*radian));
          fact1:=fact1num/fact1den;
          vc:=4*sqr(a)*sqr(sin(radian))/sqr(lambda);
              vcround:=round(vc);
          writeln(outdata,theta:5:2,radian:5:2,dspacing:5:2,qvalue:5:2

              fact0:5:2,fact1:5:2,vcround:5);
          hkl(vcround);
       end;
       close(indata);
       close(outdata);
       close(outdata1);
          writeln('FILE_OUTDATA.RES HAS BEEN CREATED');
          writeln('COMPUTATION COMPLETE')

end.
```

APPENDIX 2

The reciprocal lattice.

When calculating the angle between two lattice planes of a given indices, or in transforming the indices of a given plane or direction from those corresponding to one unit cell to those appropriate to another, it is often useful to use the reciprocal lattice, it was first developed for carrying out lattice sums and then became important tool in diffraction problems and in theory of the behaviour of electrons in crystals.

Assuming we have a crystal lattice and select a crystal lattice and select a primitive unit cell and let the translation vectors a, b and c. the three vectors reciprocal to a, b, c can be defined as a*, b* and c*. The defining relations are:

$$a^* = \frac{b \times c}{a.[b \times c]} \qquad b^* = \frac{c \times a}{b.[c \times a]} \quad \text{and} \quad C^* = \frac{a \times b}{c.[a \times b]}$$

1) A lattice vector of the reciprocal lattice such as $r^* = ha^* + kb^* + LC^*$ is normal to the planes of Miller Indices (hkl) in the real lattice. Thus h, k, l are given small integral values the vectors r* (hkl) obtained, represent the normals to low index planes.

2) The magnitude of r*, i.e. |r*|, is equal to the reciprocal of the spacing of the planes of the real lattice of Miller Indices (hkl).

From fig. A2.2

$$r^*\left(\frac{a}{h} - \frac{b}{k}\right) = (ha^* + kb^* + Lc^*).\left(\frac{a}{h} - \frac{b}{k}\right) =$$

$$\frac{ha.a^*}{h} - \frac{kb.b^*}{k} = 0$$

Thus proving (1)

To prove (2) the spacing of the lattice planes of Indices (hkl) equals the projection of a/h onto their normal. By (1) a unit vector along the normal to this plane $\frac{r^*}{r^*}$. The spacing d_{hkl} is given by

$$d_{hkl} = \frac{a}{h} \cdot \frac{r^*}{|r^*|} = \frac{ha.a^*}{h|r^*|} = \frac{1}{|r^*|}$$

where $r^* = ha^* + kb^* + lc^*$

$$\frac{1}{d_{hkl}} = r^* = ha^* + kb^* + LC^*$$

APPENDIX 3

Planar spcing

$$d_{hkl} = \frac{1}{|ha^* + Kb^* + Lc^*|}$$

Now

$$|ha^* + Kb^* + Lc^*|^2 = (ha^* + Kb^* + Lc^*).(ha^* + Kb^* + Lc^*)$$

$$= h^2a^{*2} + K^2b^{*2} + L^2C^{*2} + 2KLb^*.C^* + 2lhc^*.a^* + 2hka^*.b^*$$

$$= h^2a^{*2} + K^2b^{*2} + L^2C^{*2} + 2klb^*C^* \cos\alpha^* + 2lhc^*a^*\cos\beta^* + 2hka^*b^* \cos\gamma^*$$

where α^* is the angle between the reciporcal lattice vectors b* and c*, β^* the angle between C* and a* and γ^* the angle between a* and b*.

The interplanar spacing can be evaluated in terms of the parameters of the direct lattice by substituting for a*, b* and c*.

Therefore $\cos\alpha^* = \dfrac{\cos\beta \cos\gamma - \cos\alpha}{\sin\beta \sin\gamma}$

$$\cos\beta^* = \frac{\cos\alpha \cos\gamma - \cos\beta}{\sin\alpha \sin\gamma}$$

$$\cos\gamma^* = \frac{\cos\alpha\cos\beta - \cos\gamma}{\sin\alpha \sin\beta}$$

For simplicity

Monoclinic

Since $\alpha^* = 90^\circ$

$$d^2_{hkl} = \frac{1}{h^2a^{*2} + k^2b^{*2} + L^2C^{*2} + 2lhc^*a^* \cos\gamma^*}$$

where $\gamma^* = 180^\circ - \gamma$, $a^* = \frac{1}{a\sin\alpha}$ $b^* = \frac{1}{b}$, $c^* = \frac{1}{c\sin\gamma}$

Orthohombic

$\alpha^* = \beta^* = \gamma^* = 90^\circ$

$$d^2_{hkl} = \frac{1}{h^2a^{*2} + k^2b^{*2} + c^2C^{*2}}$$

where $a^* = \frac{1}{a}$, $b^* = \frac{1}{b}$, $c^* = \frac{1}{c}$

Trigonal

$\alpha^* = \beta^* = \gamma^*$, $a^* = b^* = c^*$

$$d^2_{hkl} = \frac{1}{[h^2 + k^2 + c^2 + 2(kl + lh + hk)\cos\alpha^*]a^{*2}}$$

Tetragonal

$\alpha^* = \beta^* = \gamma^* = 90^\circ$ $a^* = b^*$

$$d^2_{hkl} = \frac{1}{(h^2 + k^2)a^{*2} + c^2c^{*2}}$$

where $a^* = \frac{1}{a}$, $c^* = \frac{1}{c}$

Hexagonal

$$\alpha^* = \beta^* = 90^\circ, \quad \gamma^* = 60^\circ \qquad a^* = b^*$$

$$d^2_{hkl} = \frac{1}{(K^2 + h^2 + hk)a^{*2} + c^2c^{*2}},$$

where $a^* = \frac{2}{a\sqrt{3}}$, $c^* = \frac{1}{c}$

Cubic

$$\alpha^* = \beta^* = \gamma^* = 90^\circ,$$

$$a^* = b^* \quad c^*$$

$$d^2_{hkl} = \frac{1}{(h^2 + k^2 + l^2)a^*}$$

where $a^* = \frac{1}{a}$